

Modelling twentieth century global ocean circulation and iceberg flux at 48°N: implications for west Greenland iceberg discharge



David J. Wilton*, Grant R. Bigg, Edward Hanna

Department of Geography, The University of Sheffield, Sheffield S10 2TN, UK

ARTICLE INFO

Article history:

Received 14 November 2013

Received in revised form 24 June 2015

Accepted 4 July 2015

Available online 9 July 2015

ABSTRACT

We have used a coupled ocean–iceberg model to study the variation in global ocean circulation and North Atlantic iceberg flux from 1900 to 2008. The latter component of the study focused particularly on Greenland icebergs feeding into the Labrador Current and past Newfoundland. The model was forced with daily heat, freshwater and wind fluxes from the Twentieth Century Reanalysis. The reanalysis heat fluxes were shown to be offset from the, shorter, NCEP reanalysis and a grid-point correction was applied to this component of the forcing. The model produces a generally realistic ocean circulation, although with an enhanced Atlantic Meridional Overturning largely due to the forcing. The modelled iceberg flux at 48°N is well correlated with the long-term observed flux when using a modelled iceberg discharge that varies in a similar fashion to the highly variable observed flux at 48°N. From this model we infer changes in the spatial and temporal variability of iceberg calving from western Greenland. During the first third of the twentieth century the majority of modelled icebergs reaching 48°N derive from southern Greenland, while only after 1930 is the traditional perspective of a majority of such icebergs originating from Baffin Bay consistent with model results. Decadal-scale changes in the dominant regional sources are found, with oscillations between western Greenland and northern Baffin Bay. The latter origin was modelled to be most important in the last third of the twentieth century, although west Greenland sources have increased in importance in recent years. The model correctly reproduces the pronounced late spring peak in flux at 48°N for southern Greenland icebergs, but has an approximately six month offset for icebergs from Baffin Bay, most likely due to resolution issues leading to model icebergs not being delayed in shallow coastal waters, whereas in reality they may be grounded for some time or trapped in coastal sea-ice.

© 2015 The Authors. Published by Elsevier Ltd. This is an open access article under the CC BY license (<http://creativecommons.org/licenses/by/4.0/>).

1. Introduction

In this study we aim through experiments carried out with a coupled ocean–iceberg model driven with daily meteorological and oceanographic forcing data, to both examine the modelled long-term variability over the twentieth century of some key ocean circulation indicators, but also to gain an understanding of what leads to the variation in the flux of icebergs in the western Atlantic. The latter will allow us to infer likely changes to the calving rate of the Greenland Ice Sheet (GrIS) over the modelled period of 1900–2008, and long-term change in the principal calving sources of North Atlantic icebergs. It must be said at the outset of this study that there are significant limitations to what can be achieved because of the likely errors in the Twentieth Century Reanalysis Project (20CR) atmospheric forcing (Lindsay et al., 2014) and the limited nature of long-term iceberg flux data, irrespective of the quality of the ocean–iceberg model. We will return to this limiting aspect of the study in the Synthesis but believe this

work helps give an understanding of ocean and Greenland ice sheet decadal variability over the last century. Despite the focus on long-term coupled climate modelling in recent years (e.g. IPCC (2013) and a large number of recent works feeding into the IPCC Fifth Assessment Report), there is still a need to study the direct effect of analysed, rather than modelled, atmospheric processes on the global ocean.

Until the advent of the 20CR (Compo et al., 2011), atmospheric reanalysis products (e.g. from the European Centre for Medium Range Weather Forecasting and the U.S.'s National Center for Climate Prediction) covered limited time periods, at most back to 1948 (Kalnay et al., 1996). Ocean model simulations using this forcing are normally over more limited periods of years to a few decades, and often restrict attention to particular areas of the globe. Köberle and Gerdes (2007), in an unusually long integration simulated the global ocean over 1948–2003. They concentrated heavily on the Arctic Ocean variability, however, with very limited discussion of the wider modelled global circulation.

The one paper we found that attempts an ocean model simulation of a similar timescale (1900–1997) to that discussed here (but

* Corresponding author.

does not include the iceberg component) is that of Kauker et al. (2008). They used a statistical approach based on station and gridded data, to generate monthly forcing fields of sea level pressure, 10 m winds, precipitation, surface air temperature, cloudiness and surface dewpoint temperature. This relied on statistical relationships generated during an overlap period with the NCEP Reanalysis, in contrast to the 20CR, which was based on a dynamical reanalysis procedure at 3-hourly timescale. Once again Kauker et al. (2008) focus on the Arctic, although there is more discussion concerning the Atlantic and Pacific, to which we will return later. The 20CR provides estimates of global atmospheric variables at 3-hourly temporal, and approximately 2° spatial resolution, back to 1871. A global ocean simulation using this Reanalysis has not yet been published in the literature. Thus the first of our aims here is to use the 20CR to force a coupled ocean–iceberg model, the Fine Resolution Greenland and Labrador ocean model (FRUGAL) (Wadley and Bigg, 2002; Green and Bigg, 2011), in order to study the modelled, century-scale ocean circulation.

The second of our aims is related to the iceberg component of the FRUGAL model. Understanding long-term changes in the GrIS discharge is important due to implications for its contribution to future mean sea level rise (Rignot et al., 2011) and for changes to Atlantic overturning circulation as a result of freshwater input to the North Atlantic (Hu et al., 2009). Estimates of GrIS surface mass balance from a number of different methods (Hanna et al., 2011) can be related to variation in rates of precipitation and run-off, but estimates of ice loss due to ice flow over the GrIS grounding line, and ultimately as iceberg calving, are more difficult to include (Rignot et al., 2008; Bamber et al., 2012; Box and Colgan, 2013). There is strong evidence for greater mass loss in recent years (Van den Broeke et al., 2009; Velicogna, 2009; Rignot et al., 2011; Shepherd et al., 2012; Hanna et al., 2013); much of this is due to increases in melt (Rignot et al., 2011), but there have also been notable increases in ice flow over the grounding line (Rignot et al., 2011) and iceberg calving rates (Howat and Eddy, 2011). Understanding the difference between mass flow across the grounding line, which helps constrain estimates of sea-level rise attributable to Greenland (Rignot et al., 2011; Shepherd et al., 2012), and iceberg calving, which affects the freshwater supply to the ocean, is important, as icebergs release melt water directly into the oceans over a much greater area than does direct runoff from ice sheets and ice caps.

This GrIS ice discharge component of the work requires knowledge of NW Atlantic iceberg fluxes. Monthly estimates of the number of icebergs passing south of 48°N have been made by the U.S. Coast Guard's International Ice Patrol (IIP) since 1900 (Marko et al., 1994; Christensen and Luzader, 2012; Murphy and Cass, 2012). Fig. 1 shows the consequent annual iceberg total passing 48°N (I48N), and the average seasonal cycle, which has a dominant peak between March and June. Although these are estimates

obtained via different platforms evolving over time, through more than a century of data collection, they are the only long-term record of iceberg numbers in the northwest Atlantic, and regarded as the best (and only) quantitative measure of century-scale iceberg variation (Newell, 1993; Murphy and Cass, 2012; Christensen and Luzader, 2012; Bigg et al., 2014). I48N shows great interannual variability, at times changing from thousands of icebergs crossing 48°N one year to less than ten the next. This inter-annual variability must be due to both variations in the climate and ocean circulation over the northwest Atlantic/Greenland area as well as variations in calving flux from the GrIS, which must be the major source of these icebergs given the known surface ocean currents in the area (Fig. 2).

We first present more details of the data and model components of our study, and develop the experiments run to attain our aims. The results are then discussed, firstly of the global ocean simulation, then focusing on the North Atlantic component of this, before examining the details of the iceberg simulation of the I48N series, and its implications for GrIS ice discharge. The final section returns to the questions of the limitations of the study but also what we believe has been achieved in understanding both ocean and iceberg variability over the twentieth century.

2. Materials and methods

2.1. 20CR forcing data

The Twentieth Century Reanalysis Project version 2 (Compo et al., 2011), provides the forcing data needed for the ocean model. It extends from 1871 onwards; here the data from 1890 is used. It is derived, using a dynamical reanalysis procedure, from surface pressure observations alone, with observed sea-surface temperatures and sea-ice distributions as reanalysis boundary conditions. Note that this uses far less variety of observed variables as input to the reanalysis scheme than does a standard reanalysis such as NCEP (Kalnay et al., 1996). We calculated daily averages of the variables required for the ocean–iceberg model's heat, fresh water and wind fluxes at each model gridpoint. Preliminary experiments found that the heat fluxes derived without modification from the output of the 20CR gave rise to sea surface temperatures that were too high in some parts of the North Atlantic, particularly in the Labrador and Irminger Seas (Fig. 3). Another NCEP reanalysis product relying on assimilation of all available atmospheric observations (Kalnay et al., 1996), that does not cover the years prior to 1948, had previously been successfully used to provide daily FRUGAL forcing data (Bigg et al., 2005). We therefore made adjustments to the heat fluxes derived from 20CR, so that the mean value for a specific grid point over the whole period 1890–2008 was the same as the mean for the 1948–2008 NCEP/NCAR fluxes, thereby adjusting the heat fluxes downwards whilst still retaining the day-to-day variation of the 20CR (Fig. 4). The resulting fluxes are insensitive to variation of the 20CR mean period used in the adjustment and bring the sea surface temperatures much closer to expected values (Fig. 3). The one regional exception to this procedure was over the sea-ice poleward of 50°N or 63°S , where the 20CR ice mask is the same or better than NCEP's (where a common time period occurs), and so their heat fluxes are similar. In these regions the adjustment to the 20CR heat flux was capped at -50 W m^{-2} .

2.2. The FRUGAL coupled ocean–iceberg model

The Fine Resolution Greenland and Labrador ocean model (Wadley and Bigg, 2002) is specifically designed for studies focusing on the North Atlantic and Arctic. It uses a curvilinear grid with

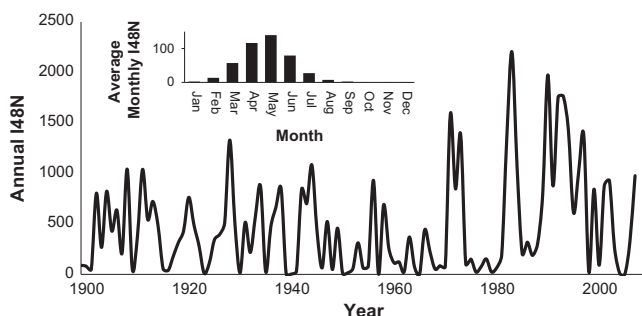


Fig. 1. Annual variation in I48N as observed by the IIP with mean monthly variation inset.



Fig. 2. Map of the Greenland and Labrador area with arrows showing the direction of ocean currents likely to be carrying icebergs towards 48°N off the Newfoundland coast. Based on iceberg drift patterns shown in Newell (1993), Marko et al. (1994) and Valeur et al. (1996).

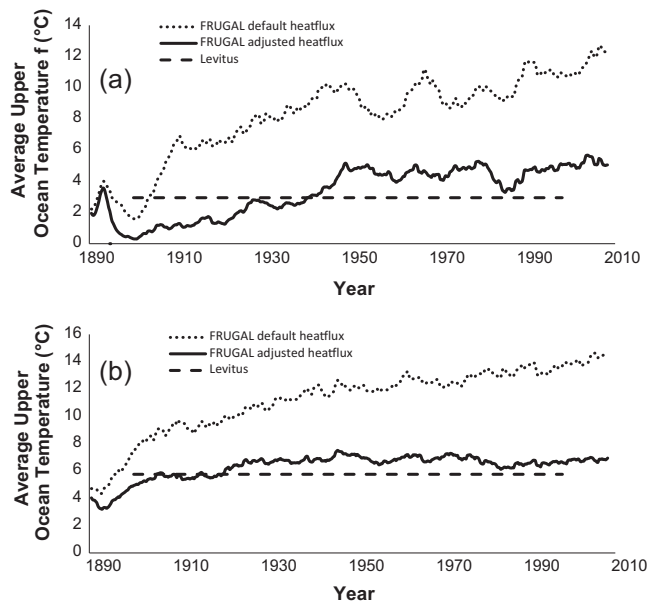


Fig. 3. Fine resolution level 1 (0–30 m depth) FRUGAL temperatures (°C), averaged over (a) the Labrador Sea, (b) the Denmark Strait and Irminger Sea. The former area is defined as between 50–65°N and 65–45°W, the latter is defined as between 60–70°N and 45–20°W. Also shown for comparison are the average 1900–1991 temperatures over the same areas and depth range from the NODC (Levitus) World Ocean Atlas, (Levitus et al., 1994).

the north pole in Greenland, giving an enhanced resolution in the Arctic and North Atlantic (Madec and Imbard, 1996). With a fine resolution grid of 182×211 cells this is equivalent to approximately 2° longitude by 1.5° latitude in the Southern Hemisphere

with a resolution of 20 km around the Greenland coast. The resolution does not coarsen to 100 km until $\sim 50^\circ$ N (Bigg et al., 2005), so the whole of the model's Arctic Ocean and large parts of the North Atlantic will be approaching eddy-permitting resolution. Time step length is a function of grid spacing to allow efficient integration of the variable resolution grid (Wadley and Bigg, 1999). FRUGAL has a free surface formulation for the barotropic mode (Webb, 1996), and 19 vertical levels varying in thickness from 30 m near the surface to 500 m at depth. Tracer (temperature and salinity) mixing has components on the horizontal, vertical and along isoneutral surfaces (Griffies et al., 1998). The values of the mixing coefficients are taken from England (1993). The topography is constructed from the ETOPO (1986) dataset, with sill depths taken from Thompson (1995). The sea-ice component of the ocean model is a thermodynamic model with simple advection (Wadley and Bigg, 2002). There are sea-ice models with more explicit physics representation available (e.g. Hibler (1979)), but as we are not focusing on Arctic sea-ice, and have significant computational burdens from the long integration period, with the addition of the data-intensive iceberg model, we have retained this simpler approach. The main drawback for our simulation of using this relatively simple sea-ice scheme is with its treatment of the physics of icebergs within sea-ice, to which we return in Section 2.4.3.

The dynamic and thermodynamic iceberg model is described in Bigg et al. (1997) and Gladstone et al. (2001), and its coupling to an ocean model in Levine and Bigg (2008). The horizontal movement of an iceberg is a function of dynamic processes: the Coriolis force, wave radiation, horizontal pressure gradient force and drag factors from the surrounding water, air and sea-ice. The thermodynamic changes to an iceberg's mass and shape are due to basal melting, buoyant convection, wave erosion and smaller terms due to sublimation and latent heat transfer. This model has been extensively

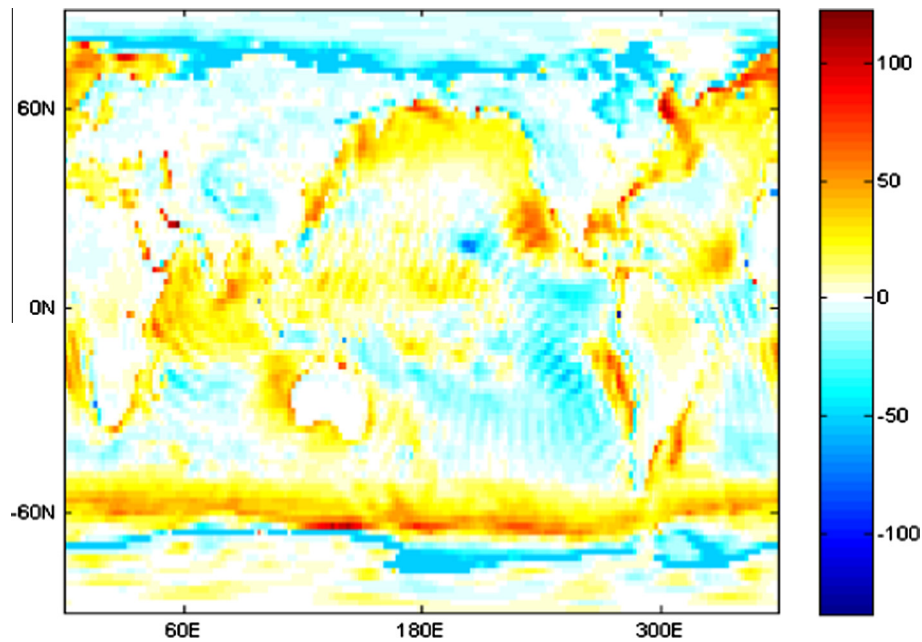


Fig. 4. The adjustment made, in Wm^{-2} , at each model gridpoint to the average 20CR net heat fluxes, through subtracting the mean NCEP heat flux for that point.

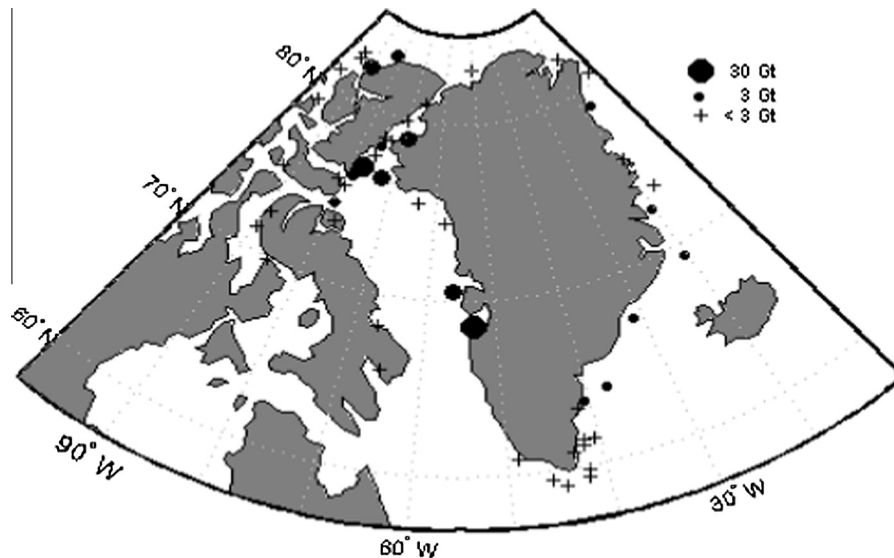


Fig. 5. Map showing Greenland regional iceberg release sites used in FRUGAL. Those sites discharging less than 3 Gt per year are shown by a '+'. Those discharging more than this are shown by a filled circle with radius indicating relative annual discharge on a logarithmic scale. There are also a further 16 release sites in the Northern Hemisphere, in Svalbard and the Russian Arctic islands, not shown.

tested for long-term integrations in the Arctic (Bigg et al., 1996; Bigg and Wilton, 2014), the Antarctic (Gladstone et al., 2001), for past climates (Levine and Bigg, 2008; Bigg et al., 2011) and been tested by comparison with marine core data (e.g. Andrews et al., 2014). It has been adapted for use in the GFDL coupled climate model (Martin and Adcroft, 2010) and the Nucleus for European Modelling of the Ocean (Marsh et al., 2015).

Model icebergs are seeded four times a year into the ocean at fixed points, with locally varying annual fluxes, according to a method described by Bigg and Wadley (2001). There are 70 seed sites in the Northern Hemisphere (Fig. 5) and 29 around Antarctica (Levine and Bigg, 2008). Seed sites may correspond to the discharge from multiple marine terminating glaciers and are positioned offshore to avoid problems with model icebergs

escaping coastal waters. Model icebergs are divided into ten different size classes, ranging from 0.491 to 492×10^9 kg in mass, based on observations of present day Arctic and Southern Ocean icebergs (Bigg et al., 1997), excluding giant icebergs. Each model berg is assigned a scale factor appropriate to that size of berg from its specific seed site. Summing the mass of each berg, multiplied by its scale factor, gives the average ice discharge per quarter year expected from that seed site, as indicated by the size of the points in Fig. 5. While estimates of grounding line ice flux in Greenland and Antarctica suggest significant recent increases (Rignot et al., 2011), for our simulation we use lower ice discharge rates compatible with the more stable mass balances of the ice sheets during the period before 1990. These are calculated assuming a balance of ice and water discharge with an atmospheric model's

mean precipitation field over the globe's ice sheets (Bigg and Wadley, 2001; Gladstone et al., 2001). If I48N iceberg fluxes are consistent with Greenland ice discharge our model should show increased fluxes in recent years, as indeed it does (see Section 3 and Bigg et al., 2014).

Previous FRUGAL ocean–iceberg model results have assumed the same number of model icebergs per seed site per quarter, with typically releases on the first days of January, April, July and October. However, here we also investigate seasonal and yearly variations in ice discharge. For investigating seasonal variation, 75% of a given year's model bergs are released in one peak month with 15% on the preceding, and 10% on the following, quarter release day, with no iceberg discharge six months after the peak. However, for the Southern Hemisphere we retain the original annual release history, as we are less concerned about iceberg impact in the less well resolved Southern Ocean in this study. The peak discharge should most intuitively correspond to the summer when iceberg calving peaks (Howat et al., 2010). However calving itself is not being modelled and we need to account for the time it might take an iceberg to get from the glacier calving front, through a fjord and its seasonal sea-ice and into the open seas where our model iceberg seed sites are located. The consequences of this parameterization of iceberg release will be discussed in more detail in the following sections. Variation in total yearly discharge is simulated by adjusting the scale factors associated with each model berg with respect to an appropriate measure of the assumed variation in discharge from tidewater glaciers.

The ocean–iceberg model is forced with heat, freshwater and wind fluxes on a daily time scale (see Bigg et al. (2005) and Condrón et al. (2008) for previous daily-forced examples of FRUGAL simulations and Section 2.1 for more detail on this forcing). Heat flux is a function of latent and sensible heat plus net long and short wave radiation, freshwater flux is the difference between precipitation and evaporation, and the wind fluxes have separate zonal and meridional components.

2.3. The I48N iceberg time series

I48N came from the IIP's iceberg counts over 1900–2008. These exclude growlers (icebergs <5 m in length). It is important for considering the issue of confidence in the quality control of this time series to understand the origin and purpose of its collation. The beginning of the formal activities of the U.S. Coast Guard's IIP was in 1913, following the loss of the RMS Titanic and 1500 lives, in 1912. From its beginning, there has been a requirement for the IIP to provide ice hazard information to the major shipping routes into eastern North America (Murphy and Cass, 2012). Missing significant icebergs entering these shipping lanes, for which crossings of the 48th parallel is a good proxy, has potentially serious consequences. For example, in the period from 1882 to 1890, 14 vessels were lost and 40 seriously damaged by collisions with icebergs (<http://www.navcen.uscg.gov/?pageName=IIPHHistory>; accessed 1/30/2013). Since the creation of the IIP there have been no serious incidents with icebergs in these waters, for vessels heeding IIP warnings (Christensen and Luzader, 2012). This fact alone speaks to the thoroughness of the surveys leading to the I48N compilation. The observational method has changed over time (Christensen and Luzader, 2012), from early records from sailing ships, specific ice patrol cruises (from 1912 and more formally 1914) through dedicated oceanographic surveys (from 1932), aircraft and ship-board radar (from the 1940s) to more recent use of models to predict the drift of icebergs seen (normally from the annual aircraft campaign) north of 48°N that then cross this latitude line. While each of these methods has its disadvantages, it is noteworthy that since the late 1950s regular patrol activities have been suspended before the end of low ice seasons because of the confidence in detection

(Christensen and Luzader, 2012). The time series has similar maxima and minima throughout, and no obvious biases during the two World Wars, despite the cessation of normal patrols during 1917–18 and 1942–45. While needing to be treated with care, the I48N series is likely to be reliable (Christensen and Luzader, 2012; Murphy and Cass, 2012).

The IIP also holds an iceberg sighting record from 1960, and to show the robustness of I48N we carried out a reconciliation between the sighting and I48N records for 1966, one of only two years in the record where the I48N time series shows no icebergs crossing 48°N during the entire season. This is reported in the Appendix A, with the conclusion being that the I48N time-series is likely to be more accurate than the raw sighting database.

2.4. Methodology

The ocean model was spun-up, without model icebergs, using the same monthly average forcing data, in this case the European Centre for Medium-Range Weather Forecasts ERA-40 reanalysis (Uppala et al., 2005) as this was known to lead to FRUGAL producing a good reproduction of the ocean circulation with daily forcing (Condrón et al., 2008), repeated for at least 300 years (1000 years for the coarse resolution version) until major ocean fluxes had converged. The model was then restarted from the spun-up state with daily average forcing data from 20CR, and model icebergs, starting from 1st January 1890. The position, velocity, mass and size of model bergs was archived every 3 months. Similar data are also recorded for each model berg that crosses a specified iceberg flux measurement line, such as at 48°N. The model also stores the date and location at which each model berg was created as it crosses these measurement lines.

We performed experiments using two contrasting spatial resolutions. The coarse model has 47×52 points, which is equivalent to 1–2° resolution in the Arctic, and the finer grid is as described in Section 2.2. The control run released icebergs uniformly throughout the year, but we also carried out a series of sensitivity experiments, described below.

2.4.1. Seasonal variation in model berg release

As described in Section 2.2 model bergs are released every three months with 75% in one peak month, for Northern Hemisphere sites. Preliminary experiments indicated model bergs from south Greenland sites, those between 59°N and 64°N, typically took 3–5 months to reach 48°N. Therefore in order that they reach 48°N in the same peak months, March to June, as the observed I48N (Fig. 1) the peak release month was taken as January. This does not correspond to the actual peak in calving, which most likely occurs in summer (Howat et al., 2010), but accounts for the time it might take an iceberg to reach our seed sites in the open seas through fjordal sea-ice (Fig. 5). For seed sites north of 64°N preliminary experiments showed it took around a year, or more, for modelled bergs to reach 48°N and that the precise peak release month does not matter as much as it does for Southern Greenland sites. Therefore, for the release sites north of 64°N we set the peak release month to mid-summer, July.

2.4.2. Annual variation in total ice discharge

One of the main aims of this work is to shed light on the annual variation in calving from the GrIS; we reflect this in the model by varying the total amount of ice discharged annually. We incorporate this variability into the model by varying the scaling factors associated with each model berg. We used the observed I48N to modify the individual model berg's scale factors, $f(y)$, according to

$$f(y) = (I48N(y)/I48N_m)f \quad (1)$$

where f is the original scale factor for the model berg, y is the year, $I48N(y')$ is the observed iceberg flux at 48°N for year y' , $I48N_m$ is the mean $I48N$ from 1900 to 2008, and y' is the appropriate year to scale by, as established by the preliminary experiments. For iceberg seed sites in Southern Greenland, south of 64°N , $y' = y$ since bergs from that region reaching 48°N tend to do so in the same year. For seed sites north of 64°N , $y' = y + 1$ as bergs from further north, whose peak release month is July, take around a year or more to reach 48°N .

2.4.3. Sea-ice drag tests

Although the FRUGAL model does simulate sea-ice (Wadley and Bigg, 2002) that then has a drag effect on model bergs (Bigg et al., 1997), it is known that this drag representation is too weak in thick or high concentration sea-ice (Lichey and Hellmer, 2001). Therefore, we also carried out an additional sensitivity experiment using the fine resolution model with a crude enhancement to the default sea-ice effect to see if this was the root of a problem we shall see later with the arrival times of bergs of a more northerly origin at 48°N . In this scheme, where the model level 1 gridbox temperature was $<0^\circ\text{C}$ (this is not sea surface temperature, but represents the mean temperature of the top 30 m) we reduced the velocity of the model bergs to 10% of the value they would otherwise have from the iceberg model equations. This is clearly an approximation, and will not necessarily reflect actual sea-ice distributions accurately, but it gave us a way to investigate the effect of enhanced sea-ice drag in likely pack ice zones. This parameterization is not fully conserving of momentum, but gives a first-order approximation to the enhanced drag effect found by Lichey and Hellmer (2001). A more sophisticated scheme to that described below has been used by Hunke and Comeau (2011) for modelling the sea-ice interactions of a few individual icebergs in the Weddell Sea, but we are here interested only in whether this sea-ice effect explains the timing issue mentioned and not the path of individual icebergs.

3. Results and discussion

In this section we will concern ourselves with the details of the finer resolution model simulation, as this is what will be used almost exclusively in later sections. The general behaviour of the coarser resolution model is, however, similar.

3.1. Main features of the modelled twentieth century ocean circulation

Fig. 3 showed the magnitude, and variability, of some North Atlantic upper ocean temperature fields and we will explore the behaviour of the model in this region more fully in Section 3.2.

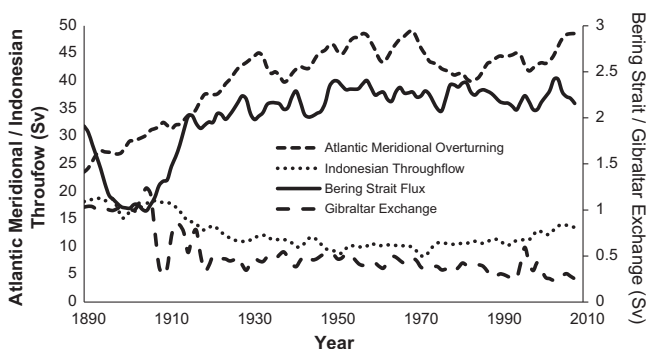


Fig. 6. Annual mean fluxes (in Sv) of main components of the modelled global overturning circulation, 1890–2008: Atlantic Meridional Overturning; Indonesian Throughflow; Bering Strait Flux; Gibraltar exchange.

However, we begin by examining variability in some of the main characteristics of the global meridional circulation. Fig. 6 shows the variability in the annual mean Atlantic meridional overturning circulation (AMOC), the linking flows from the Pacific through the Indonesian Throughflow and the Bering Strait, and also the strength of the exchange at the Strait of Gibraltar. Note that the latter is explicitly represented in the model, but as a wider strait than the 15 km reality. Because the exchange is forced by hydraulic control, ocean models can successfully resolve one-grid wide flows at larger than actual scales (Wadley and Bigg, 1996). Rogerson et al. (2010) have shown that FRUGAL's scheme is successfully able to reproduce the modern estimates of ~ 1 Sv (Bryden et al., 1994) using climatological forcing; the mean flow here is less, at 0.5 ± 0.2 Sv. Note that after an initial adjustment period of ~ 20 years, there is little evidence of trend in this exchange, although there is interannual variability. The overturning indices of the AMOC and the Indonesian Throughflow take an additional decade to equilibrate, but then also show significant interannual variability but only weak trends, if any, over the remainder of the simulation. Note that the mean AMOC peak towards the end of the series of ~ 46 Sv is over double the magnitude of observations at this time at 26.5°N (Cunningham et al., 2007). A previous, shorter FRUGAL simulation with daily NCEP fluxes led to interannual variability more in the 20–25 Sv range (Bigg et al., 2005), so it is likely that the enhanced AMOC is at least partly due to the 20CR forcing fields. Indeed, a sample of snapshot meridional cross-sections of the AMOC (Fig. S1) shows that there is a local enhancement of the AMOC around 20 – 30°N leading to the high peak values, most likely due to the lack of success of the flux adjustment scheme in the North Atlantic sub-tropics (Fig. 7).

The Indonesian Throughflow has a wide range of observed fluxes, from 8 to 15 Sv (Wijffels and Meyers, 2004); the simulation's Throughflow, 12.5 ± 3 Sv (Fig. 6), is at the upper end of this range. Similarly, the observed Bering Strait inflow of ~ 1 Sv (Woodgate et al., 2012) is a half that shown in Fig. 6, 2.0 ± 0.4 Sv, although FRUGAL's value is within 1 Sv. At the large scale outside the Atlantic, therefore, the fine-resolution model run has flows similar to observed, but with a stronger global overturning than is supported by observations. We will return to this point in the next section when we consider the North Atlantic more closely.

3.2. The modelled northern Atlantic during the twentieth century

Here we will examine the characteristics of the modelled northern Atlantic to determine whether the strong modelled AMOC has significant consequences for the remainder of the paper, where we focus on the properties of the modelled iceberg flux from Greenland and so a very specific, and limited, area of the NW Atlantic.

Fig. 3 has already shown that the general upper ocean temperature in the northern Atlantic is within 1 – 2°C of the mean observed temperature. Even some of the significant, shorter-term changes in the model, such as the $>0.5^\circ\text{C}$ drop in temperature through the 1980s in the Labrador Sea matches observations (Dickson et al., 1996). The general trend since 1950, however, is for the modelled SST to be fairly stable in both regions shown in Fig. 3. Turning to variables possibly more affected by the enhanced AMOC we show the average modelled regional ocean fluxes across the Nordic Seas in Fig. 8, as well as their time series over 1890–2008. On average, there is a net 2 Sv modelled flow from the Atlantic into the Arctic through the Nordic Seas. This is very similar to recent inverse method calculations (Tsubouchi et al., 2012) and within the range of uncertainty of earlier estimates (Goldner, 1999). However, the details of the modelled circulation are rather different, particularly for those fluxes into the Arctic.

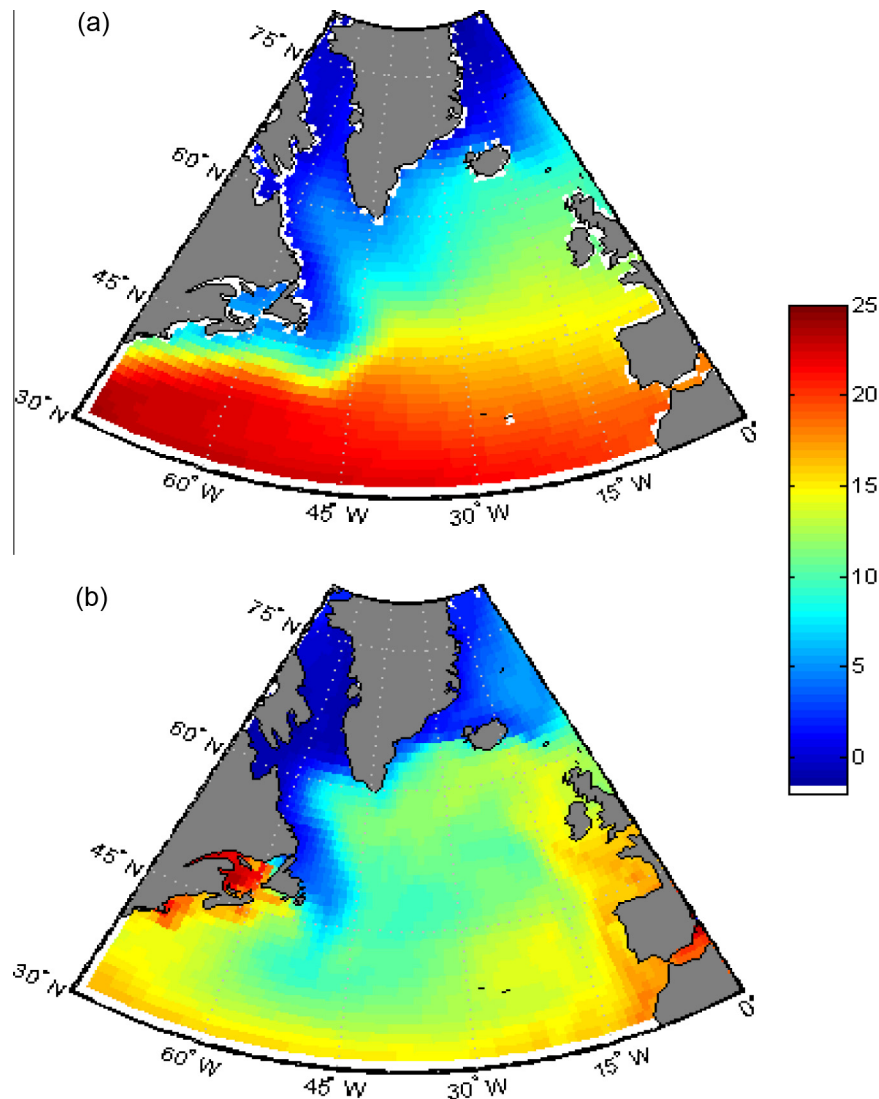


Fig. 7. Mean upper ocean temperature fields over the NW Atlantic for 1900–1991: (a) climatological upper ocean temperature 0–30 m depth, from [Levitus et al. \(1994\)](#); (b) model level 1 (0–30 m depth) mean.

[Fig. 8](#) shows net mass transfer into the Arctic through the Fram Strait and net mass loss from the Arctic into the Barents Sea. This is opposite to the conventional view of fluxes into the Arctic from the Nordic Seas. [Tsubouchi et al. \(2012\)](#) show exactly the opposite fluxes, namely 3.6 Sv entering the Arctic through the Barents Sea and 1.6 leaving through Fram Strait. What has occurred in the model is an enhancement of the sub-surface West Spitsbergen Current, so that the model's mass, while correct in magnitude, predominantly enters the Arctic, at depth, further west than it should. The upper level flow southwards through the Fram Strait ($\sim 1\text{--}1.8$ Sv over 1930–2000) is similar to observations. This behaviour has been found also in a previous daily-forced FRUGAL simulation ([Bigg et al., 2005](#)). Nevertheless, the fluxes across the Greenland–Iceland–Scotland Ridge are compatible with observations. Historical fluxes into the Nordic Seas between Iceland and Scotland were estimated at 5.3 Sv (see [Wadley and Bigg \(2002\)](#) for details), but more recent estimates have placed this closer to 7.5–8.5 Sv ([Orvik et al., 2001](#); [Rossby and Flagg, 2012](#)). The current model, with 6.1 ± 0.4 Sv, falls close to more historical estimates. The observed Denmark Strait volume flux is much better observed, but is highly variable from year to year ([Bacon, 1998](#)). While the

mean southward flow in the second half of the twentieth century is ~ 6.5 Sv, it varies over 2.5–8.5 Sv, with half of the observations within 1 Sv of the modelled mean of 4.1 ± 0.4 Sv. Thus, the exchange between the Atlantic and the Nordic Seas is likely to be 1–2 Sv too weak, but the modelled means fall within the observational spread. Note also that while the modelled fluxes have significant decadal-scale variability there is little suggestion of long-term trends beyond the initial adjustment period ([Fig. 8](#)).

We now consider the western North Atlantic, where most of our later attention will be focused because of the Greenland iceberg flux. The mean upper ocean temperature field for the region over 1900–1991 is shown in [Fig. 7](#), along with the model mean level 1 field, both of which correspond to the upper 0–30 m. The modelled ocean temperature shows general agreement with [Levitus et al. \(1994\)](#), as far as the regions important to I48N in the northern and NW Atlantic are concerned. However, the model upper ocean temperature south of about 45°N tends to be too cool by several °C and ~ 2 °C too warm off the British Isles in the eastern Atlantic. The heat flux adjustment, Section 2.1, has clearly helped in the northern Atlantic ([Fig. 3](#)), but been less successful further south, leading to the enhancement of the AMOC ([Fig. S1](#)).

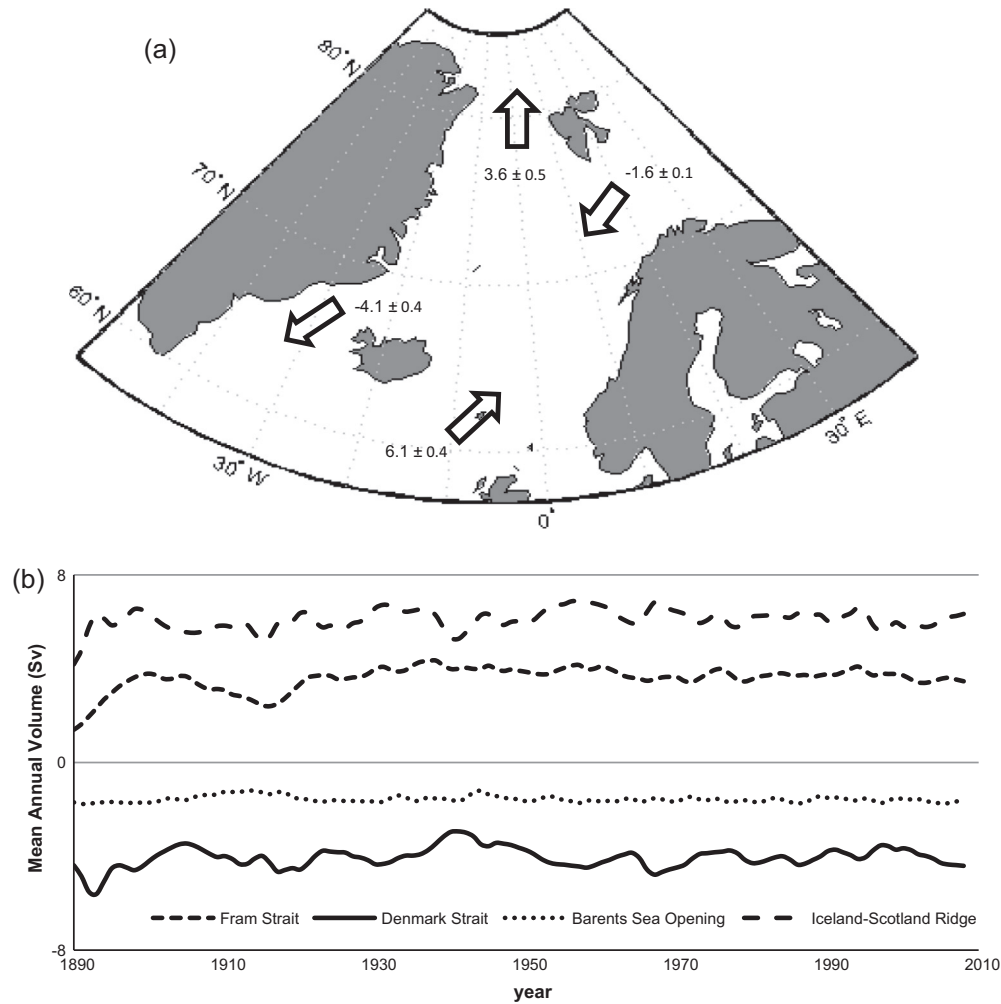


Fig. 8. Mean fluxes, in Sv, across the two main entrances to the Nordic Seas from the Atlantic (Denmark Strait and Iceland–Scotland ridge) and the Arctic (Fram Strait and the Barents Sea): (a) overall average for 1890–2008; (b) time series of individual annual mean fluxes.

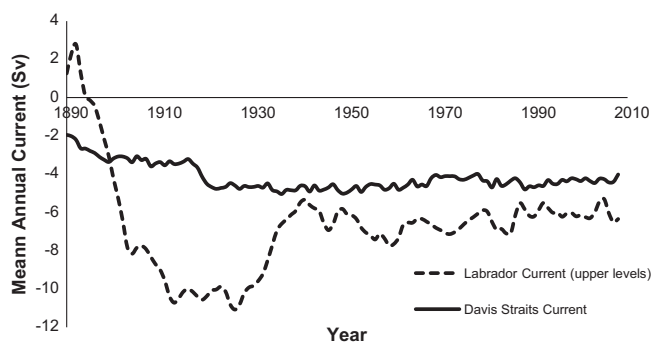


Fig. 9. Annual mean of model Labrador and Davis Strait currents. The Labrador Current is defined as the flux southwards across 52°N from the Labrador coast 15° eastwards above 251 m (model levels 1–4). The Davis Strait current is defined as the total flux southwards across the model grid between West Greenland and Baffin Island, at ~66°N.

The basic flux through the Canadian Archipelago and out through the Davis Strait into the North Atlantic is a key indicator for the iceberg modelling. Earlier estimates placed this around 1.3 Sv (Goldner, 1999) but more recent estimates suggest it is closer to double this (2.3 ± 0.7 Sv in Curry et al. (2011) and 2.6 ± 1.0 Sv in Cuny et al. (2005)). For the model (Fig. 10) this can be estimated as 4.5 ± 0.3 Sv, from 1930 to 2008 (pre 1920 it is noticeably lower). This is ~2 Sv higher than the observed

estimates. Half of this over-estimation is because the additional model flux through the Bering Strait (Fig. 6) flows into the Atlantic through the Canadian Archipelago. The other major current in the region is the Labrador Current, running along the coast southwards off Labrador and beyond. After the adjustment period the model Labrador Current is high (Fig. 9), around 10 Sv, but this drops to a mean of 6.4 ± 0.4 Sv after 1940. It is difficult to exactly match the model calculation with the varied observational estimates of the Labrador Current but most of the latter measured off Newfoundland are near 6 Sv (Petrie and Buckley, 1996; Dengler et al., 2006; Han et al., 2008) and so comparable to the model flux.

In summary, the model generally performs reasonably well in the northern Atlantic, particularly in the Northwest. An exception to this is in the deep water flow of the Atlantic sector of the Arctic. The Atlantic as a whole has an enhanced AMOC as well, but overall we have confidence in the 20CR forcing having led to an ocean circulation fit for examining the general properties of the long-term GrIS iceberg flux variability. This confidence is further enhanced by agreement of the model's iceberg record in the Denmark Strait with twentieth century ice-rafter debris core records (Andrews et al., 2014), and its performance in predicting the likely origin of the iceberg that collided with the RMS Titanic in 1912 (Bigg and Wilton, 2014). We therefore next turn to the properties of the iceberg modelling.

3.3. Modelled I48N with constant yearly iceberg discharge

Both the coarser and finer resolution models with a constant yearly discharge do not reproduce well the interannual variation of the observed I48N series (Fig. 10, dotted lines, $r = -0.03$ for coarse and $r = 0.11$ for fine), although the coarser resolution model's iceberg number flux has a mean annual total of 501, similar to that of the observed, 476. Nevertheless, it has a long-term decreasing trend whereas the long-term trend of the observed I48N is reasonably constant throughout most of the twentieth century, with a sharp increase towards the end. For the finer resolution results with constant yearly discharge the annual average iceberg mean is well below the observed (95). These results clearly show that an ocean–iceberg model assuming constant yearly discharge of icebergs from Northern Hemisphere ocean terminating glaciers does not lead to the observed flux at the key exit point from the Labrador Sea of 48°N. Meteorological variations over, and ocean circulation responses within, the oceans are not sufficient to explain the observed variation in icebergs numbers south of 48°N. This therefore indicates – in line with independent observations for the modern satellite record (Howat and Eddy, 2011; Seale et al., 2011) – that we should assume some degree of variation in annual discharge of icebergs from Greenland, and perhaps, other Northern Hemisphere marine-terminating glaciers.

3.4. Modelled I48N with variable yearly iceberg discharge

When the model iceberg flux is scaled according to Eq. (1), based on the observed I48N, we see that the coarser resolution model results match the observed I48N very well (Fig. 10, bold). Qualitatively the match is very good indeed with peaks and troughs mostly coinciding between model and observed ($r = 0.92$). However, we will see in the next section that the coarser resolution model is right for the wrong reasons. The finer resolution simulation with variable yearly discharge likewise gives a good qualitative match ($r = 0.83$) but underestimates the observed by a significant amount in most years. This, however, is not

unexpected. There are 70 Northern Hemisphere seed sites for model icebergs, with 27 of these being along the Greenland coast (Fig. 5). Whilst many of these sites represent multiple marine-terminating glaciers they do not cover all outlet glaciers of the GrIS and the total mass of ice discharged each year on average from Greenland sites is the same as for the constant discharge model, i.e. 96 Gt yr^{-1} from Greenland sites. The average iceberg discharge from the GrIS, at least that estimated before 1990 and so during the period before Greenland began responding strongly to global warming (Hanna et al., 2012), is, however, around 270 Gt yr^{-1} (Baur, 1968; Reeh, 1985, 1994; Bigg, 1999). More recent estimates are up to double this (e.g. Rignot et al., 2011; Bamber et al., 2012) but have been made during this warming phase and so we felt are unlikely to be in equilibrium. Therefore, we should reasonably scale up our model I48N, but we choose a factor of $270/96$ here, to match the pre-2000 estimates. However, this may be an under-estimate. If we do this scaling for the finer resolution results (Fig. 11), we now see a better quantitative match between model and observed, with a mean model annual value of 305. However, the model peaks are noticeably not as high as the observed, especially before 1960, and not all the high I48N years observed from the 1990s onwards are reproduced by the model. This is likely to be due to regional variation in peak discharges, even though the high correlation suggests that there is a general, Greenland-wide, tendency for similar interannual variability (as imposed by Eq. (1)). Exploring this fully is beyond the scope of this paper, but we speculate on regional variation in the Synthesis.

3.5. Iceberg source variation

In addition to considering the magnitude of modelled iceberg flux at 48°N we also consider the source of the model icebergs. Table 1 shows variations from four source regions, South Greenland, Mid West Greenland and South Baffin Island, North West Greenland and the Canadian Arctic, and an “Other” category, incorporating East Greenland sources, as well as the Svalbard and Russian Arctic islands. The results pre- and post-1930 are shown separately in Table 1 as there is a distinct change in the dominant source area around this time. The interannual variability in I48N source is shown for the finer resolution results in Fig. 12.

I48N in the coarser model simulations is dominated by South Greenland sources, with a significant minority from the “Other” category, most of which are not of Greenland origin. There is virtually no contribution from West Greenland. Both the lack of a West Greenland contribution and the rather high Svalbard and Russian contributions for the coarse resolution are inconsistent with the pattern of ocean currents in the area (Fig. 2) as well as with the limited past mapping of iceberg density patterns (Wolford, 1981; Newell, 1993; Valeur et al., 1996). The lack of contribution from West Greenland is due to the low spatial resolution, resulting in model bergs being unable to pass readily through the 2–3 grid

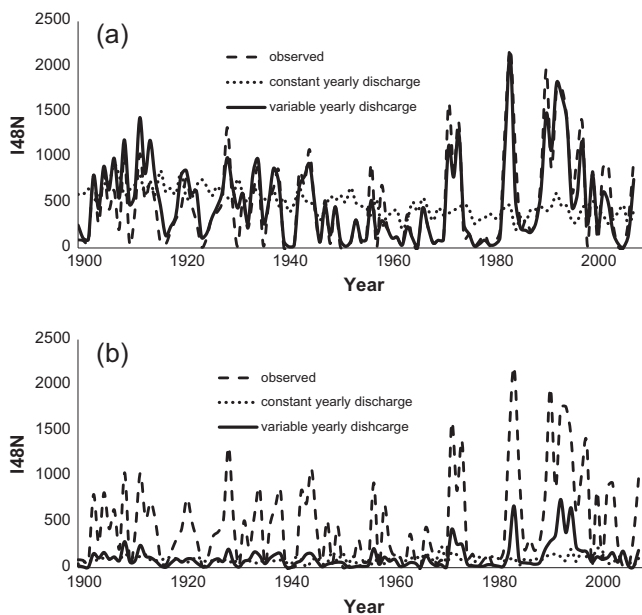


Fig. 10. Annual model I48N compared with observed. Each panel shows the annual observed I48N (dashed), modelled I48N using the same yearly discharge distribution throughout the simulation (grey) and the modelled I48N using variable yearly discharge (bold), whose magnitude varies as given by (1). (a) Gives the coarse resolution model results; (b) the fine resolution results.

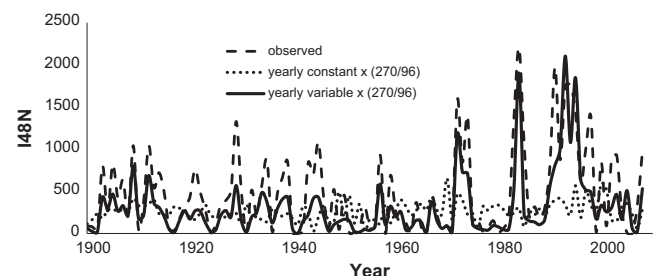


Fig. 11. Fine resolution results scaled to account for average discharge from the whole GrIS.

Table 1

Percentage model I48N contribution from model release sites in four regions of Greenland, and elsewhere.^a

Range of years	Model resolution	Annual discharge	South	Mid West	North West	Other
1900–1930	Coarser	Constant	70.8	0.5		28.7
		Variable	70.4	0.0		29.6
	Finer	Constant	83.7	9.1	6.6	0.6
		Variable	83.9	10.5	5.4	0.2
1931–2008	Coarser	Constant	76.1	0.9		23.0
		Variable	79.6	0.5		20.0
	Finer	Constant	33.9	23.4	42.6	0.1
		Variable	34.0	20.1	45.3	0.5

^a South is those icebergs from below 65°N. Mid West is those released between 65°N and 72°N on the West coast of Greenland or Baffin Island (although the latter do not, in fact, contribute to I48N). North West is all other release sites in Baffin Bay, Nares Strait and the Canadian Arctic islands north of 72°N, but not discharging icebergs to the Arctic. The 'other' category includes all of Eastern Greenland above 65°N together with sites in Svalbard and the Russian Arctic islands. For the coarser model the Mid and North West categories are merged.

point-wise Davis Strait because of the lack of a clear southward current along the western side of the Strait. Fig. 13a shows the average density of model icebergs for the coarser model. We can clearly see high density in North Baffin Bay, and enhanced density within the main Bay, but little evidence of a trail exiting through Davis Strait, thus demonstrating the lack of a southward current in the coarser model here.

Fig. 13a also shows why icebergs originating from South Greenland, and the Nordic Seas, dominated the coarser model results shown in Table 1. There is a clear path flowing almost directly towards 48°N, but crossing this parallel quite a long way east of Newfoundland. The high contribution from the Eastern Arctic in the coarser model is again a result of the low resolution leading to a poorly modelled North Atlantic with currents carrying model bergs from the high Arctic too far south. Again Fig. 13a shows this with a moderately high density in the Greenland Sea and Fram Strait stretching south of 70°N, some of which is flowing

through the Denmark Strait, or even occasionally to the east of Iceland, and ultimately joining the flux of model bergs from South Greenland to 48°N. The coarser model simulation clearly fails to capture the movement of icebergs around Greenland that we would expect from Fig. 2, particularly with respect to those from West Greenland. It also does not have many model bergs from South Greenland being advected northwards along the west Greenland coast, where they might cross the northern Labrador Sea (Fig. 2 and Marko et al. (1994)) to be entrained in the Labrador Current and travel on to 48°N by this route. This means a great many coarser resolution simulation bergs from South Greenland can reach 48°N via a shorter route across the central Labrador Sea and therefore have more chance of reaching 48°N before they melt. As a final reason for not believing the coarser resolution results, both marine core evidence from the Holocene, and the finer resolution model results, suggest icebergs in the Denmark Strait are largely of local origin with little material/icebergs originating from further north (Andrews et al., 2014). For all these reasons, and the inflating impact of the scaling for net Greenland discharge previously discussed, we believe the coarser resolution simulation results of Fig. 13a show believable results for the wrong reasons.

Turning now to the finer resolution simulations, Table 1, and Figs. 12b and 13, show that, for the twentieth century as a whole, over half of the model bergs composing I48N originate from the west coast of Greenland, a significant number come from South Greenland and virtually none are from East Greenland or further afield. Before 1930, the modelled I48N is dominated by icebergs of South Greenland origin (Table 1, Fig. 12b). During this time a clear area of non-zero iceberg density is seen stretching from the South of Greenland down through the Labrador Sea to 48°N and beyond (Fig. 13b). However, although the actual density per grid cell is low, bergs are spread over a wide area. There is a clear area of no icebergs at all off the southwest of Greenland. This indicates that the contribution to I48N from South Greenland in the finer model is made up of icebergs heading directly for the Labrador coast over a fairly wide area, rather than being taken northwards up the West Greenland coast and then crossing the Davis Strait to join the Labrador Current off Baffin Island. We can see that within Baffin Bay icebergs are concentrated to the North and that there is relatively low density spreading through the Davis Strait, hence leading to the relatively small contribution to I48N from the West of Greenland.

After 1930, the contribution to I48N from the west coast becomes dominant, but around a third of the icebergs still originate from South Greenland (Fig. 12b). Of the west coast icebergs, ones of Northwest origin are usually more prevalent, which is particularly so for those years with a very high total I48N (Fig. 12b), while the Mid-West contribution is very variable from year to year. However, from around 2000 onwards the Northwest contribution almost disappears (Fig. 12b). The change in iceberg origin is seen when comparing Fig. 13b and c. In Fig. 13c there is still an area of non-zero iceberg density due south of Greenland but this is spread over a smaller area than it was before 1930 (Fig. 13b), and there are now modelled icebergs off the southwest coast, heading north and crossing the Labrador Sea just south of Davis Strait, as suggested in the schematic of suspected iceberg tracks shown, for example, in Marko et al. (1994). There is a clear stream of relatively high density 2–4 grid cells wide from the South of Baffin Island, along the Labrador coast and onto Newfoundland. This corresponds to the route we would expect icebergs from the West of Greenland to take to 48°N. We also see icebergs concentrated around the coasts of Baffin Bay, but also more spread out over the full extent of the Bay and into the Davis Strait, as suggested by the limited observations from the 1960s–90s (Wolford, 1981; Valeur et al., 1996).

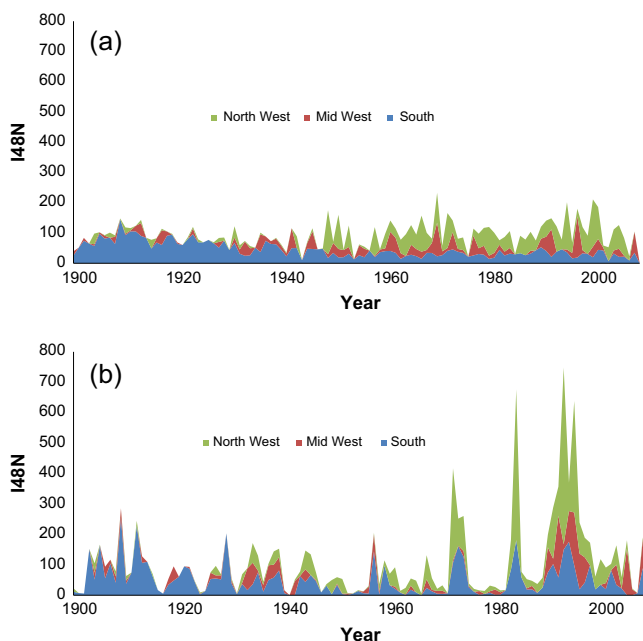


Fig. 12. Variation in Greenland source region for the finer resolution model I48N. Different regions are defined in Table 1. "Other" category not shown as its contribution is negligible. (a) Constant yearly discharge; (b) variable yearly discharge, as determined by (1).

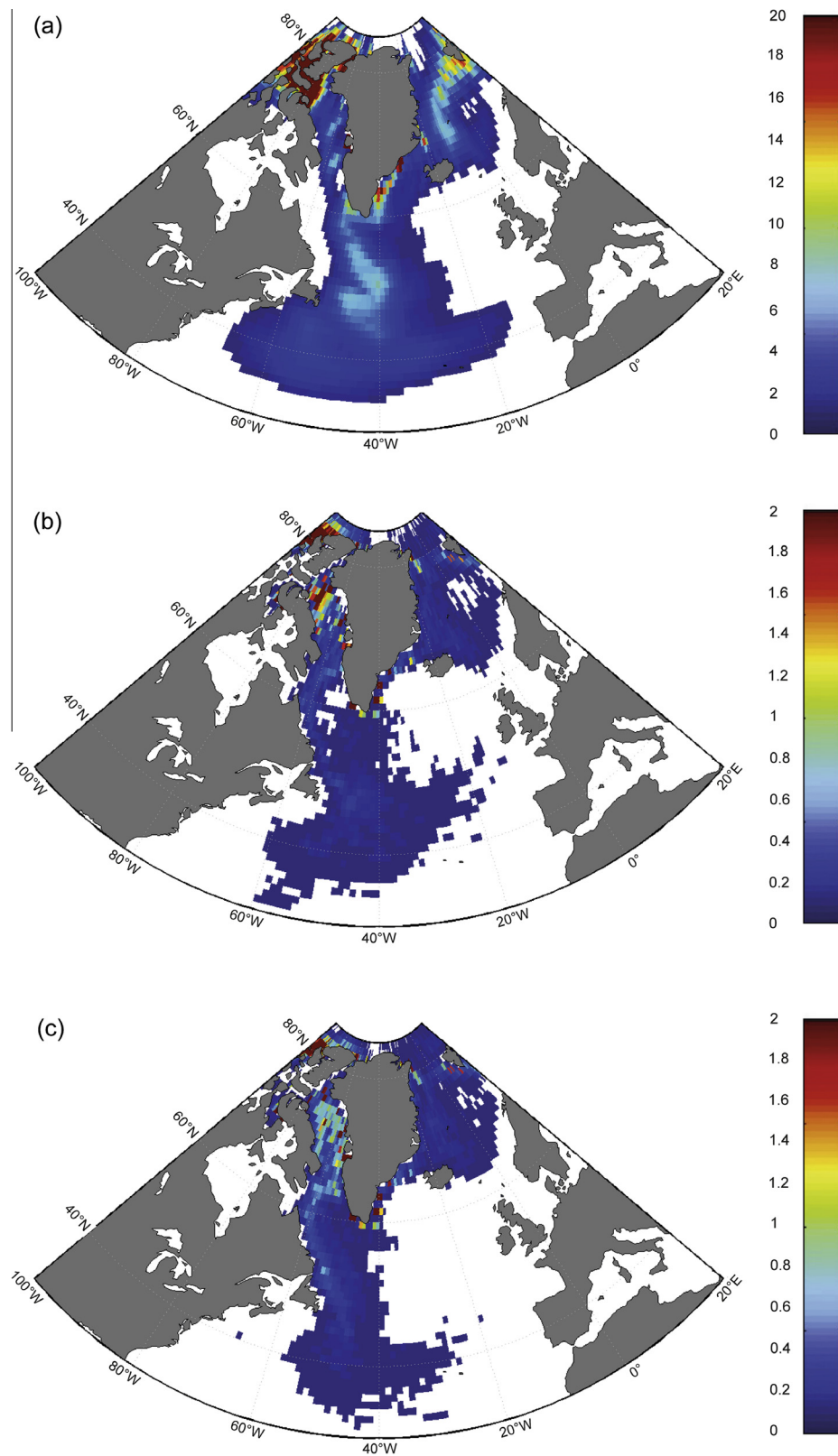


Fig. 13. Average iceberg densities over the North Atlantic in terms of number of icebergs per model grid cell, interpolated to a longitude–latitude grid. Densities shown are capped at an appropriate upper limit for each graph, as those grid cells that include iceberg release sites may have iceberg densities very much higher than the maximum shown. (a) Coarser resolution model densities, averaged over 1900–2008; (b) finer resolution model densities, averaged over 1900–1930; (c) Finer resolution model densities, averaged over 1931–2008.

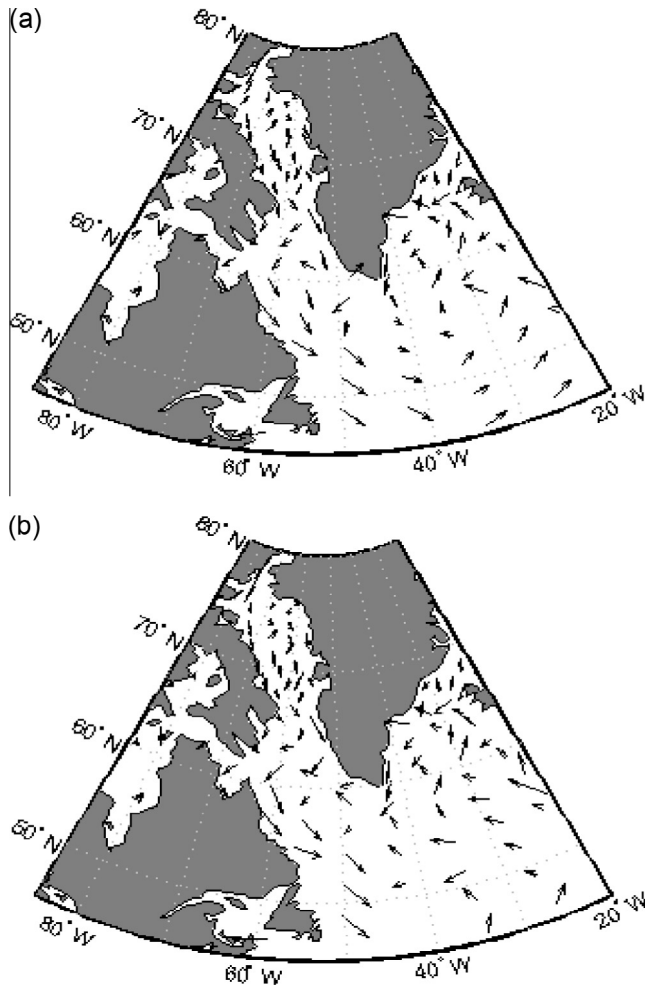


Fig. 14. Mean ocean currents from 45 m depth (level 2) for the finer resolution model with variable yearly discharge, (a) 1900–1930 and (b) 1931–2008. Arrows are plotted from the coordinates of where the current is calculated (5 model grid points apart), pointing in the direction of flow with length proportional to the square root of the magnitude.

Examination of the local ocean currents (Figs. 14 and S2) shows how these change leading to the differences in the iceberg density fields, and modelled sources of I48N, pre- and post-1930. Before 1930, a mean southward coastal current off the mid to southwest coast of Greenland, extending towards the southern tip of Greenland, is modelled (Fig. 14a). Thus, modelled South Greenland bergs are not generally advected northwards in this era, as they mostly would be if the currents were as expected from later reconstructions (Fig. 2). They instead just flow south and southwest towards Newfoundland and are therefore more likely to reach 48°N than if they took a longer route initially northwards. There is, however, a modelled southwards current along the Labrador coast (Fig. 14a). Therefore, those few model bergs from West Greenland that get through Davis Strait are advected in the right direction to enable them to reach Newfoundland. However, as shown in Figs. 9 and S2, the southwards currents within Baffin Bay that would bring icebergs through the Davis Strait are relatively weak.

For the post-1930 currents (Fig. 14b) we see a contrasting situation. The southwards current through the Davis Straits, around 66°N, is stronger and Fig. 9 clearly shows the annual Davis Straits current increasing from around 1920. The southwards coastal current on the West coast of Greenland does not extend much further south than Davis Strait, in contrast to its behaviour

pre-1930. The dominant current near southern Greenland is north-westwards into the Labrador Sea, rather than the previous southwards flow. Hence, on average, after 1930 icebergs from South Greenland can be taken northwards, with the possibility of then being entrained in southward currents in the Labrador Sea, taking them in the direction of Newfoundland. They are therefore less likely to reach 48°N than the icebergs from pre-1930 that take a more direct, due south, route. This change in trajectory is clearly seen in the modelled mean time for South Greenland icebergs to reach 48°N: it changes from a relatively rapid 108 ± 59 days prior to 1930 to 142 ± 49 days since then. It is therefore changes to the currents in the Labrador Sea and Baffin Bay that produce the modelled change in the major sources of I48N after 1930. Pre-1930 there are stronger modelled southwards currents from South Greenland, thereby leading to the higher proportion of I48N from South Greenland sources, and weaker southwards currents in Baffin Bay, thereby leading to the lower proportion of I48N from West Greenland sources, as reflected in the analysis shown in Table 1 and Fig. 12. We will return to the significance of this change around 1930 in the Synthesis.

3.6. Seasonal variation

There is reasonable agreement between the finer resolution model and observed annual I48N (Fig. 11), but we should also consider the seasonal variation of the model iceberg flux at 48°N to see if the clear peak in the observed flux from March to July (Fig. 1) is reproduced. Fig. 15a shows the mean seasonal cycle of the model iceberg flux, including separate contributions from South and West Greenland, and compares this with the observed seasonal cycle. Model icebergs reaching 48°N from South Greenland arrive with a similar seasonal distribution to those observed. Note that these modelled bergs agree exactly with the (persistent) observed peak month of May for the period 1931–2008. However, prior to 1930, the model peak month for bergs originating from South Greenland is March, with a significant contribution in April. This agrees with the above noted change over the twentieth century in mean time taken to reach 48°N in the model, but suggests that more of the pre-1930 modelled icebergs from South Greenland reached 48°N via a shorter route than would have in reality.

Model icebergs originating from further north along western Greenland tend, however, to arrive from October to January (Fig. 15a), and therefore be ~6 months out of phase with the observations. This is not a consequence of when most West Greenland model bergs are released, i.e. July, as the same peak arrival period of October to January for icebergs of West Greenland origin was found in another simulation with constant discharge throughout the year. The precise date of their release into the model is clearly unimportant. What is therefore governing the date at which the icebergs of west Greenland origin cross 48°N is either the speed at which they travel through the Labrador Sea or the timing of their exit through the Davis Strait.

The presence of sea-ice will affect both of these properties (Marko et al., 1994), and a drag on iceberg motion due to sea-ice is included in FRUGAL (Bigg et al., 1997). However, this scheme does not have sufficient drag in high ice concentration areas (Lichey and Hellmer, 2001) and an analysis of the modelled sea-ice distribution shows that the latter is significantly more patchy in Baffin Bay, Davis Strait and off the Labrador coast than in observations (Parkinson and Cavalieri, 2008). This underestimation of sea-ice means that model icebergs will not be slowed down by sea ice as much as they should. This could lead to model icebergs from the West of Greenland reaching 48°N too quickly, and so at the wrong time of year. In order to test this hypothesis to explain the seasonal arrival timing of bergs from Northwest and Mid-west Greenland, we re-ran the finer resolution model, applying a first

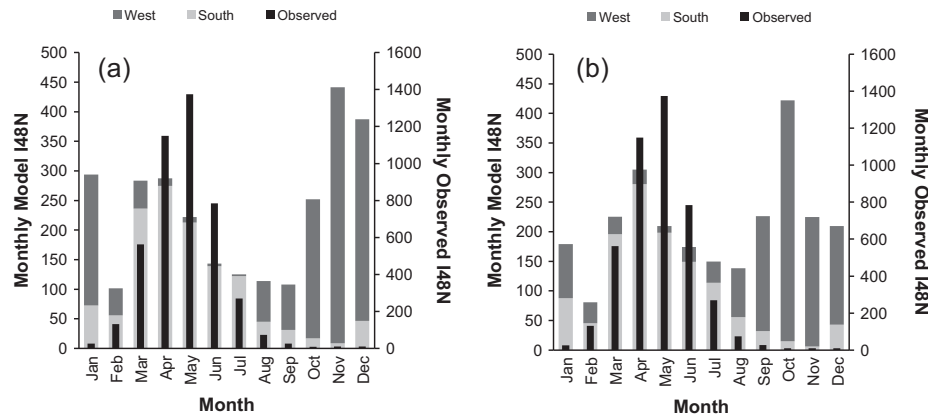


Fig. 15. Seasonal variation in finer resolution model iceberg flux at 48°N (bars), with variable yearly ice discharge, compared to that for the observed I48N (bold lines). Average monthly flux (1900–2008) is shown split, for model results, into contributions from West and South Greenland areas, as defined for Table 1. (a) Variable yearly ice discharge according to (1); (b) as for (a) but with the enhanced sea-ice drag parameterization.

order parameterization of an enhanced sea ice drag (see Section 2.4.3). The resulting seasonal variation of model iceberg flux is shown in Fig. 15b. Model icebergs from West Greenland, with this sea-ice drag parameterization, do arrive at 48°N a month or two earlier in the year compared to the standard simulation (Fig. 15a), but not sufficiently so to match the observed data, and the overall model correlation with the observed I48N declines significantly (from $r = 0.83$ to 0.63). This appears to suggest that increasing the sea-ice drag paradoxically speeds up the passage of Baffin Bay icebergs to 48°N. However, what has actually happened is that the new sea-ice parameterization has pushed back the arrival peaks for both the Mid-west and Northwest regions within Baffin Bay by multiples of approximately a year (Fig. 16) and made little difference to the seasonal timing of the exit from Baffin Bay.

Given the difference in seasonal cycle that still persists between the model bergs of Baffin Bay origin and the observed I48N, there must be other factors responsible for this discrepancy. There are three candidates for the responsible mismatch. One of these is the accuracy of the details of model surface temperature fields along the Labrador and Newfoundland coast. The surface temperature of the Labrador Sea is usually above 0 °C, in the model, except for a narrow region just off the coast. The modelled icebergs are mainly further offshore than this (Fig. 13c) and therefore the sea-ice parameterization is unlikely to be activated for model bergs in the Labrador Sea.

Another candidate is the ocean circulation along this coast. If we re-examine Figs. 13b and S2 we see that the stream of modelled iceberg density from the Davis Strait to Newfoundland is well clear of the coast. Records of actual icebergs in this area show (see any annual International Ice Patrol report at <http://www.navcen.uscg.gov/?pageName=IIPAnnualReports>) many icebergs much closer to the coast that often become grounded in shallow coastal waters (Newell, 1993) or are diverted into the Strait of Belle Isle, towards the Gulf of St. Lawrence (Huntsman et al., 1954). That is not happening in the model since the icebergs are not getting close enough to the coast, and even if they did the spatial resolution of the coastline is not high enough to resolve the bays and islands where icebergs tend to ground. Therefore this provides a plausible explanation for model bergs embedded in the near-coastal part of the Labrador Current reaching 48°N too quickly, and so at the wrong time of year.

The third possible explanation is that the icebergs are escaping through the Davis Strait at a common, but incorrect time of year, which is more dependent on current than sea-ice variability. They should be leaving Baffin Bay in the autumn, at the time of

minimum sea-ice, and reaching Newfoundland next spring. The total model iceberg flux into Davis Strait from Baffin Bay does have a peak, as expected, in the late summer and autumn (Fig. 17). However, only a small fraction of this iceberg flux reaches 48°N, and analysis of these particular model icebergs shows that they predominantly entered Davis Strait earlier in the year, with peak exit months of May to July (Fig. 17), and took an average of 171 ± 61 days to travel from 66°N to 48°N, leading to the offset in the seasonal distribution of model I48N (Fig. 15a). Given that the scaled model I48N (Fig. 11) has a good qualitative, and reasonable quantitative, match with the observed series it seems likely the size of the iceberg flux entering Davis Strait and ultimately reaching 48°N is at least approximately correct. However, these icebergs flow in a stream too far off the Labrador coast (Fig. 13c) and therefore do not experience the delaying effects due to sea-ice and shallow coastal waters to which real icebergs are susceptible. Therefore, this resolution issue seems the most plausible explanation of why model icebergs from the West of Greenland arrive at 48°N in the wrong season. Further evidence to support this can be found in comparison to a higher-resolution (0.1°) ocean model over Baffin Bay and the Labrador Sea (Wu et al., 2012). This shows a strong southwards upper ocean current well offshore in the Labrador Sea, which FRUGAL also shows, but smaller scale upper ocean currents westwards towards the Labrador coast inshore of the main southwards current, which FRUGAL does not reproduce at the resolution used here. The latter small-scale currents would clearly be responsible for bringing icebergs in the main current towards the coastline where they might be delayed through grounding.

4. Synthesis and conclusions

We have used the FRUGAL coupled ocean–iceberg model and the daily average 20CR reanalysis to look at global ocean circulation during the twentieth century, and particularly tried to explain the observed iceberg flux in the western Atlantic. The methodology producing the 20CR reanalysis, using just surface pressure observations in the dynamical analysis (Compo et al., 2011), has been found to have some problems with its heat flux, particularly in the northern Atlantic and Southern Ocean (Fig. 4). However, adjusting the heat flux for the off-set from more comprehensive reanalysis products leads to an ocean forcing providing a more realistic ocean circulation, albeit with an overturning circulation double the strength it should have in the subtropics of the North Atlantic. In some of the circulation measures shown (Figs. 3, 6

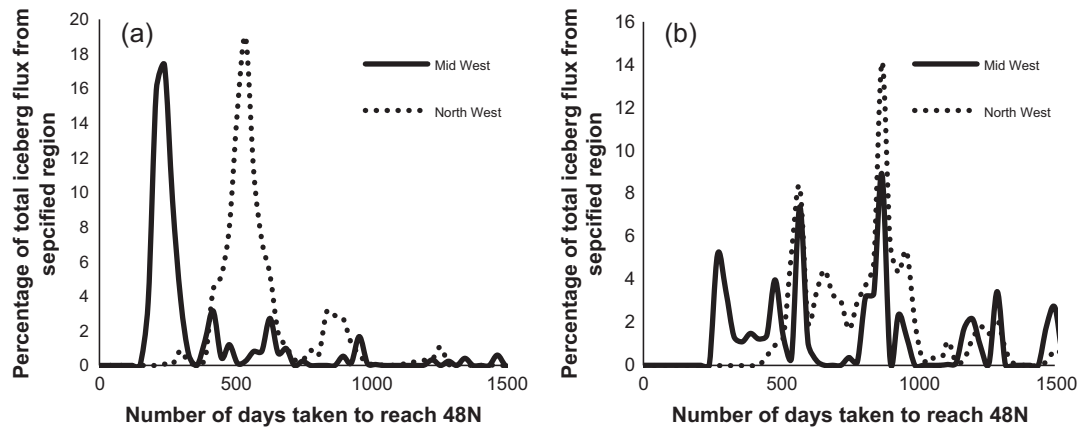


Fig. 16. Distribution of model times taken for icebergs to reach 48°N from West of Greenland. These are shown up to 1500 days only for clarity, but there are a few model icebergs taking many more years to eventually reach 48°N. (a) Variable yearly ice discharge according to (1); (b) as for (a) but with the enhanced sea-ice drag parameterization.

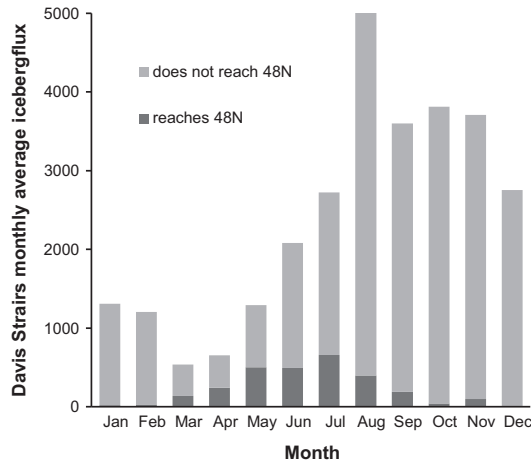


Fig. 17. Seasonal variation in finer resolution model iceberg flux through the Davis Straits, measured at 66°N. Average monthly fluxes 1900–2008 are split into that part which eventually reaches 48°N and that part which does not.

and 8) there is significant decadal-scale variability, but general stability over the century. However, some elements show a response to the global warming of the first half of the century (the Labrador Current, the Fram Strait flux, the Gibraltar exchange and the Indonesian Throughflow), while others show a response to the later twentieth century warming (AMOC, Indonesian Throughflow, Denmark Strait).

For the main purpose of our study, namely to examine through modelling the variability in GrIS discharge over the twentieth century, the finer resolution model produces an adequate circulation in the northern Atlantic, particularly in the NW Atlantic where the simulated icebergs of interest are found (Section 3.2). Both the main volume fluxes in this area, which will determine the iceberg trajectories, and the sea surface temperature, which will affect their melting rates, give us confidence in the first order properties of the ocean–iceberg model. The model variability over the twentieth century will depend crucially on the accuracy of the wind forcing of the 20CR. While this is difficult to measure during the first half of the century because of the paucity of station observations in the NW Atlantic, using the 20CR over the same time period as the ECMWF Reanalysis for calculating the surface mass balance of Greenland (Hanna et al., 2011) has shown a similar result to this well regarded reanalysis. It is noteworthy, however, that the main

change in major properties of the model, around 1930, occurs before the major increase in surface and upper air observations dating from the International Geophysical Year in 1958 and later.

Turning to the core focus of the study – the western Atlantic iceberg flux – the ocean–iceberg model, at the finer spatial resolution, can only realistically simulate the observed annual I48N if it is assumed that annual ice discharge from the GrIS varies in the same fashion as I48N. Therefore, climatological changes, as reflected in the C20R forcing data for the model, do not account for the variability in I48N and we must assume a highly variable GrIS discharge occurred across the century, at least in western and southern Greenland. We have confidence in the robustness of the approach taken to produce a first order variation of GrIS iceberg discharge not only because of the well correlated reproduction of the I48N time series ($r = 0.83$), but also because of the independent comparison with marine core ice-rafted debris records in the Denmark Strait (Andrews et al., 2014).

Available recent observations of iceberg calving flux from Greenland show significant year-to-year discharge variability in particular locations (Csatho et al., 2008; Seale et al., 2011). Reconstructions of GrIS mass loss affecting sea level based on interior ice sheet changes, rather than direct iceberg flux measurements, show significant change on a decadal-scale over the ice sheet as a whole (Rignot et al., 2008, 2011; van den Broeke et al., 2009; Box and Colgan, 2013), although not with such variation as I48N. The surface mass balance of the GrIS is not well correlated with I48N (Hanna et al., 2011). The large-scale ice dynamics leading to sea level change respond more evenly with time than does the actual calving discharge. It is to be expected that the details of calving events at particular glaciers will depend more on a range of factors, rather than just ice sheet-scale dynamics (Straneo et al., 2013), and an accurate prediction of I48N is being investigated separately using non-linear system identification modelling forced by a range of glaciological, oceanic and atmospheric factors (Bigg et al., 2014; Zhao et al., 2015). However, this paper has demonstrated a number of important points, some of which question established perceptions prevalent in the literature, but based on limited evidence, on the source of icebergs crossing 48°N and the routes they can take (Marko et al., 1994; Newell, 1993; Valeur et al., 1996).

The finer resolution modelling (Table 1) strongly suggests that icebergs passing Newfoundland come almost exclusively from southern or western Greenland (the latter term here also includes Baffin Bay sources generally). The very limited number of model icebergs derived from eastern Greenland, or beyond, is consistent

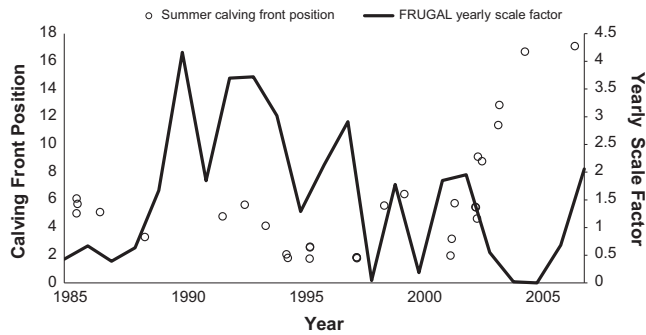


Fig. 18. Plot of change in Jakobshavn Isbrae calving front position measured up-glacier (Csatho et al., 2008) against yearly discharge scale factors used in FRUGAL for release sites at or above the latitude of Jakobshavn Isbrae, over 1985–2006.

with Denmark Strait Holocene IRD records of Andrews et al. (2014). The modelling also suggests that, while I48N may be a first order proxy for western GrIS iceberg discharge, there is considerable interannual, and longer-term, variability in the origin of the icebergs reaching 48°N.

For the first 30 years of the twentieth century, modelled icebergs making up I48N predominantly originated from southern Greenland, while thereafter Mid-west and Northwest Greenland contributed approximately two thirds of the I48N flux (Table 1; Fig. 12). These sub-centennial changes in source were due to changes in ocean circulation. Such a change in origin is also consistent with a more easterly route of the icebergs to 48°N, and the weaker correlation between I48N and winter Newfoundland coastal sea ice extent (Hill and Jones, 1990) before 1930 compared to afterwards (0.61 compared with 0.79 for 1931–70). There is also evidence of early twentieth century changes to the behaviour of glaciers in the Mid West of Greenland, with respect to their changes in length (Leclercq et al., 2012). Many land-terminating glaciers in this area show increased temporary rates of retreat from around 1930 onwards, or sometimes earlier, linked with the Early Twentieth Century Warm Period in Greenland (Hanna et al., 2012), although a subsequent slowdown probably occurred as conditions cooled once again around 1950. Therefore, if similar changes happened to marine-terminating glaciers, then there may have been an increase in the Mid-west contribution to I48N due to increases in calving rate as well as the changes due to ocean circulation we modelled.

The higher frequency variability suggested by the model in Fig. 12, with decadal-scale switches in the importance of the three main release sites, is less easy to confirm because there are limited long-term measurements of glacier discharge. However, an intermittent record of calving front location at the major mid-west Greenland marine-terminating glacier in Jakobshavn Isbrae since 1944 does exist (Csatho et al., 2008). For the first 40 years of this record there are relatively few data points, most of which show small change, which is consistent with the generally smaller modelled fluxes from this period, and particularly the low Mid-west contribution to the total (Fig. 12). However, more observations are available from 1985 onwards. A fixed calving front position from year to year is consistent with a similar annual discharge, while a rapid retreat suggests an increase in flux and an advance is compatible with a reduced flux. The interannual variation in the contribution of Jakobshavn Isbrae to I48N would therefore be expected to show some degree of correlation with the change of the calving front position, albeit possibly a year or two out of phase since we vary model iceberg discharge from West Greenland according to the following year's observed I48N and some model bergs from this region may take two or more years to reach 48°N (Fig. 16).

We show, in Fig. 18, the scale factors for annual discharge used in FRUGAL according to Eq. (1), for release sites at or above the latitude of Jakobshavn Isbrae, from 1985 to 2006 alongside the summer calving front position from Csatho et al. (2008). The calving front retreats between 1991 and 1992, could correspond to the increase in calving, and therefore an increase in the scale factors, for 1993 and 1994. There are also periods of calving front retreat in 2001–2003 corresponding to a peak in the scale factors. The calving front then appears to be stable from 2004 to 2006 but if, as noted by Csatho et al. (2008), ice velocity has speeded up then this too would imply high calving flux, which we see in our scale factors for 2007. Therefore, despite the 3000 km of ocean travel, and melting, between release point and 48°N, there is consistency between rates of glacier change, particularly when large, and the signal in I48N. This gives confidence in the general character and interannual variability of our model results, and so about relating the regional variability of GrIS iceberg discharge to the decadal-scale variation in Fig. 12.

At the seasonal timescale, while the FRUGAL ocean–iceberg model is consistent with respect to likely travel times from southern Greenland, and an annual release of icebergs from the fjord mouth following winter sea ice break-up (Bigg and Wilton, 2014), despite summer calving peaks (Howat et al., 2010), it fails to bring icebergs originating in Baffin Bay to 48°N for the seasonal peak. There are likely to be a variety of causes of this offset, relating to inaccuracies in details of model circulation and temperature in the Labrador Sea. However, the main reason is likely to be due to model resolution meaning that the main stream of modelled iceberg flux is too far off the Labrador coast and therefore model bergs are not experiencing delays due to the presence of sea ice and being trapped in coastal waters. However, the presence of icebergs from several calving years in the I48N mix, particularly from north-west Greenland, is likely to be correct.

Overall then, the 20CR forcing leads to an ocean model circulation that is acceptable but not as good as studies using the more comprehensive reanalysis fields such as ECMWF or NCEP. It has, however, led to a model of iceberg flux in the NW Atlantic well correlated with I48N only if there is a strong interannual variability in Greenland calving, and long-term change in dominant iceberg sources from southern to western Greenland. As the iceberg model is now being incorporated into some major climate models (Martin and Adcroft, 2010; Marsh et al., 2015) this raises the possibility of reasonable simulation of future ocean change through better incorporation of distant iceberg melting as Greenland melting, and iceberg discharge, accelerates over the coming decades.

Acknowledgments

Funding was provided by the Natural Environmental Research Council (NERC) Grant NE/H023402/1. The International Ice Patrol I48N dataset is available at their web site <http://www.navcen.uscg.gov/?pageName=IIPIcebergCounts>. 20th Century Reanalysis V2 data and the Levitus ocean temperature data were provided by the NOAA/OAR/ESRL PSD, Boulder, Colorado, USA, from their Web site at <http://www.esrl.noaa.gov/psd/>. Support for the Twentieth Century Reanalysis Project dataset is provided by the U.S. Department of Energy, Office of Science Innovative and Novel Computational Impact on Theory and Experiment (DOE INCITE) program, and Office of Biological and Environmental Research (BER), and by the National Oceanic and Atmospheric Administration Climate Program Office. NCEP Reanalysis data was provided by the NOAA/OAR/ESRL PSD, Boulder, Colorado, USA, from their Web site at <http://www.esrl.noaa.gov/psd/>. We would like to thank BADC, and through them, ECMWF, for allowing us to access the ECMWF Reanalyses.

Appendix A

Reconciliation of the International Ice Patrol's (IIP) iceberg sighting and I48N databases for 1966

Annual reports of the IIP have been issued since 1913, and copies from the season of 1922 onwards are readily available through the Biodiversity Heritage Library (<http://www.biodiversitylibrary.org/>; see <http://archive.org/details/reportofinternat1013unit> for reports of 1923–26). A random sampling of reports during the past 90 years leaves a strong impression of a professional and careful service, sampling the ice distribution as thoroughly as the resources available allowed. Even in the early days this consisted of at least two dedicated vessels making regular surveys during the ice season. Later in the series regular monthly charts of iceberg sightings are provided, but even in the 1922 report (IIP, 1923) monthly lists of position of icebergs are provided during the peak observing period of February to July.

From 1960 a database of iceberg sightings is available (NSIDC, 1995). To demonstrate how the sighting and I48N records reconcile the records for one year, 1966, are examined here. This is a very notable year in the I48N record, being one of only two years (with 2006) in the entire record, and the only year (Fig. 1) in the twentieth century, where no icebergs are recorded crossing 48°N. This statement – of no icebergs crossing 48°N – is strongly made in the relevant annual report (Murray, 1967). However, there are 40 reports of icebergs in the sightings database south of 48°N during 1966. Growlers make up 27 of these records, and hence are not included in I48N, and one other is an unconfirmed radar target with no visual confirmation. The abundant growler collection in March south of 48°N is mentioned in the annual report (Murray, 1967). This still leaves 12 sightings, which could be included within I48N if correct. While there is no description of quality control carried out on the sightings database when the seasonal report was being prepared, there is circumstantial evidence to suggest this has happened. The 1966 report (Murray, 1967) shows an iceberg map for 24th March, only three days prior to observation 528 (from NSIDC (1995)) of a large iceberg at 47.0°N, 52.75°W. As this location is less than 10 km from the coast, some 60 km south of St. Johns in Newfoundland, it is very unlikely that an iceberg would not have appeared on the chart 3 days before. This is probably an incorrect latitude report, or a mistaken size identification of one of the growlers reported in the same area on the same day. Errors in location or identification certainly occur. The next, medium, iceberg recorded on the 4th April is placed in Placentia Bay on the south coast of Newfoundland (~47.6°N, 54.1°W), and may even be placed on Long Island in this Bay. It is inconceivable for a berg to have reached this location without having passed 48°N some weeks earlier and again, from the positions of other icebergs observed on the day, there appears to have been an error in latitude reported. The medium iceberg reported on 15th April also is likely to have a latitude error, as it is reported off the southwest coast of Newfoundland. Such errors in position are very likely in 6 of the remaining 9 records. The last records, for 12–13th June, are all in the same area (~47.8°N, 48.8°W). Despite being recorded in the database as large icebergs there is a specific comment in the annual report (Murray, 1967) mentioning this cluster, but saying that there was no aircraft confirmation of their presence and that the observations were most likely of growlers. From this brief analysis of one year it can be seen that the principal quality control has been put into the I48N series, and the annual reports, rather than the raw sighting data. We therefore suggest that I48N is likely to be one of the most robust, century-long, integrative environmental datasets available.

Appendix B. Supplementary material

Supplementary data associated with this article can be found, in the online version, at <http://dx.doi.org/10.1016/j.pocean.2015.07.003>.

References

- Andrews, J.T., Bigg, G.R., Wilton, D.J., 2014. Sediment transport from the glaciated margin of East Greenland (67–70°N) to the N Iceland shelves: detecting and modelling changing sediment sources. *Quaternary Science Reviews* 91, 204–217.
- Bacon, S., 1998. Decadal variability in the outflow from the Nordic seas to the deep Atlantic Ocean. *Nature* 394, 871–874.
- Bamber, J., van den Broeke, M., Ettema, J., Lenaerts, J., Rignot, E., 2012. Recent large increases in freshwater fluxes from Greenland into the North Atlantic. *Geophysical Research Letters* 39, L19501.
- Baur, A., 1968. Nouvelle estimation du bilan de masse de l'Inlandsis du Groenland. *Deep Sea Research* 14, 13–17.
- Bigg, G.R., 1999. An estimate of the flux of iceberg calving from Greenland. *Arctic, Antarctic and Alpine Research* 31, 174–178.
- Bigg, G.R., Dye, S.R., Wadley, M.R., 2005. Interannual variability in the 1990s in the northern Atlantic and Nordic Seas. *Journal of Atmosphere and Ocean Science* 10, 123–143.
- Bigg, G.R., Levine, R.C., Green, C.L., 2011. Modelling abrupt glacial North Atlantic freshening: rates of change and their implications for Heinrich events. *Global and Planetary Change* 79, 176–192.
- Bigg, G.R., Wadley, M.R., Stevens, D.P., Johnson, J.A., 1996. Prediction of iceberg trajectories for the North Atlantic and Arctic Oceans. *Geophysical Research Letters* 23, 33587–33590.
- Bigg, G.R., Wadley, M.R., Stevens, D.P., Johnson, J.A., 1997. Modelling the dynamics and thermodynamics of icebergs. *Cold Regions Science and Technology* 26, 113–135.
- Bigg, G.R., Wei, H., Wilton, D.J., Zhao, Y., Billings, S.A., Hanna, E., Kadirkamanathan, V., 2014. A century of variation in the dependence of Greenland iceberg calving on ice sheet surface mass balance and regional climate change. *Proceedings of the Royal Society of London A: Mathematical, Physical and Engineering Sciences* 470, 20130662.
- Bigg, G.R., Wilton, D.J., 2014. The iceberg risk in the Titanic year of 1912: was it exceptional? *Weather* 69, 100–104.
- Bigg, G.R., Wadley, M.R., 2001. The origin and flux of icebergs released into the Last Glacial Maximum Northern Hemisphere oceans: the impact of ice-sheet topography. *Journal of Quaternary Science* 16, 565–573.
- Box, J.E., Colgan, W., 2013. Greenland ice sheet mass balance reconstruction. Part III: marine ice loss and total mass balance (1840–2010). *Journal of Climate* 26, 6990–7002.
- Bryden, H.L., Candela, J., Kinder, T.H., 1994. Exchange through the Strait of Gibraltar. *Progress in Oceanography* 33, 201–248.
- Christensen, E., Luzader, J., 2012. From sea to air to space, a century of iceberg tracking technology. *Coast Guard Proceedings of the Marine Safety and Security Council* 69, 17–22.
- Compo, G.P., Whitaker, J.S., Sardeshmukh, P.D., et al., 2011. The twentieth century reanalysis project. *Quarterly Journal of the Royal Meteorological Society* 137, 1–28.
- Condron, A., Bigg, G.R., Renfrew, I.A., 2008. Modeling the impact of polar mesocyclones on ocean circulation. *Journal of Geophysical Research – Oceans* 113, C10005.
- Csatho, B., Schenk, T., van der Veen, C.J., Krabill, W.B., 2008. Intermittent thinning of Jakobshavn Isbrae, West Greenland, since the little ice age. *Journal of Glaciology* 54, 131–144.
- Cunningham, S.A., Kanzow, T., Rayner, D., Baringer, M.O., Johns, W.E., Marotzke, J., Longworth, H.R., Grant, E.M., Hirschi, J.J.M., Beal, L.M., Meinen, C.S., Bryden, H.L., 2007. Temporal variability of the Atlantic meridional overturning circulation at 26.5 degrees N. *Science* 317, 935–938.
- Cuny, J., Rhines, P.B., Kwok, R., 2005. Davis Strait volume, freshwater and heat fluxes. *Deep-Sea Research Part I* 52, 519–542.
- Curry, B., Lee, C.M., Petrie, B., 2011. Volume, freshwater, and heat fluxes through Davis Strait, 2004–05. *Journal of Physical Oceanography* 41, 429–436.
- Dengler, M., Fischer, J., Schott, F.A., Zantopp, R., 2006. Deep Labrador current and its variability in 1996–2005. *Geophysical Research Letters* 33, L21S06.
- Dickson, R., Lazier, J., Meincke, J., Rhines, P., Swift, J., 1996. Long-term coordinated changes in the convective activity of the North Atlantic. *Progress in Oceanography* 38, 241–295.
- England, M.H., 1993. Representing the global-scale water masses in ocean general circulation models. *Journal of Physical Oceanography* 23, 1523–1552.
- ETOPO, 1986. Global 5' x 5' Depth and Elevation. National Geophysical Data Center, NOAA, Boulder, Colorado, USA.
- Gladstone, R.M., Bigg, G.R., Nicholls, K.W., 2001. Iceberg trajectory modeling and meltwater injection in the Southern Ocean. *Journal of Geophysical Research – Oceans* 106, 19903–19915.
- Goldner, D.R., 1999. On the uncertainty of the mass, heat, and salt balance of the Arctic Ocean. *Journal of Geophysical Research – Oceans* 104, 29757–29770.
- Green, J.A.M., Bigg, G.R., 2011. Impacts on the global ocean circulation from vertical mixing and a collapsing ice sheet. *Journal of Marine Research* 69, 221–244.

- Griffies, S.M., Gnanadesikan, A., Pacanowski, R.C., Larichev, V.D., Dukowicz, J.K., Smith, R.D., 1998. Isoneutral diffusion in a z-coordinate ocean model. *Journal of Physical Oceanography* 28, 805–830.
- Han, G.Q., Lu, Z.S., Wang, Z.L., Helbig, J., Chen, N., de Young, B., 2008. Seasonal variability of the Labrador current and shelf circulation off Newfoundland. *Journal of Geophysical Research – Oceans* 113, C10013.
- Hanna, E., Huybrechts, P., Cappelen, J., Steffen, K., Bales, R.C., Burgess, E., McConnell, J.R., Steffensen, J.P., Van den Broeke, M., Wake, L., Bigg, G.R., Griffiths, M., Savas, D., 2011. Greenland Ice Sheet surface mass balance 1870 to 2010 based on twentieth century reanalysis, and links with global climate forcing. *Journal of Geophysical Research – Atmospheres* 116, D24121.
- Hanna, E., Mernild, S.H., Cappelen, J., Steffen, K., 2012. Recent warming in Greenland in a long-term instrumental (1881–2012) climatic context: I. Evaluation of surface air temperature records. *Environmental Research Letters* 7, 045404.
- Hanna, E., Navarro, F.J., Pattyn, F., Domingues, C., Fettweis, X., Ivins, E., Nicholls, R.J., Ritz, C.J., Smith, B., Tulaczyk, S., Whitehouse, P., Zwally, J., 2013. Ice-sheet mass balance and climate change. *Nature* 498, 51–59.
- Hibler, W.D., 1979. A dynamic thermodynamic sea ice model. *Journal of Physical Oceanography* 9, 815–846.
- Hill, B.T., Jones, S.J., 1990. The Newfoundland ice extent and the solar cycle from 1860 to 1988. *Journal of Geophysical Research* 95, 5385–5394.
- Howat, I.M., Box, J.E., Ahn, Y., Herrington, A., McFadden, E.M., 2010. Seasonal variability in the dynamics of marine-terminating outlet glaciers in Greenland. *Journal of Glaciology* 56, 601–613.
- Howat, I.M., Eddy, A., 2011. Multi-decadal retreat of Greenland's marine-terminating glaciers. *Journal of Glaciology* 57, 389–396.
- Hu, A., Meehl, G.A., Han, W., Yin, J., 2009. Transient response of the MOC and climate to potential melting of the Greenland ice sheet in the 21st century. *Geophysical Research Letters* 36, L10707.
- Huntsman, A.G., Bailey, W.B., Hachey, H.B., 1954. The general oceanography of the Strait of Belle Isle. *Journal of the Fisheries Research Board of Canada* 11, 198–260.
- Hunke, E.C., Comeau, D., 2011. Sea ice and iceberg dynamic interaction. *Journal of Geophysical Research – Oceans* 116, C05008.
- International Ice Observation and Ice Patrol Service in the North Atlantic Ocean, 1923. Season of 1922. Bulletin No. 10, U.S. Coast Guard, Washington D.C.
- IPCC, 2013. Climate change 2013: The physical science basis. In: Stocker, T.F., Qin, D., Plattner, G.-K., Tignor, M., Allen, S.K., Boschung, J., Nauels, A., Xia, Y., Bex, V., Midgley, P.M. (Eds.), Contribution of Working Group I to the Fifth Assessment Report of the Intergovernmental Panel on Climate Change. Cambridge University Press, Cambridge, United Kingdom and New York, NY, USA, 1535 pp.
- Kalnay, E., Kanmitsu, M., Kistler, R., Collins, W., Deaven, D., Gandin, L., Iredell, M., Saha, S., White, G., Woollen, J., Zhu, Y., Chelliah, M., Ebisuzaki, W., Higgins, W., Janowiak, J., Mo, K.C., Ropelewski, C., Wang, J., Leetmaa, A., Reynolds, R., Jenne, R., Joseph, D., 1996. The NCEP/NCAR 40-year reanalysis project. *Bulletin of the American Meteorological Society* 77, 437–470.
- Kauker, F., Köberle, C., Gerdes, R., Karcher, M., 2008. Modeling the 20th century Arctic Ocean/sea ice system: reconstruction of surface forcing. *Journal of Geophysical Research – Oceans* 113, C09027.
- Köberle, C., Gerdes, R., 2007. Simulated variability of the Arctic Ocean freshwater balance 1948–2001. *Journal of Physical Oceanography* 37, 1628–1644.
- Leclercq, P.W., Weidick, A., Paul, F., Bolch, T., Citterio, M., Oerlemans, J., 2012. Historical glacier length changes in West Greenland. *The Cryosphere* 6, 1339–1343.
- Levine, R.C., Bigg, G.R., 2008. Sensitivity of the glacial ocean to Heinrich events from different iceberg sources, as modelled by a coupled atmosphere-iceberg-ocean model. *Paleoceanography* 23, PA4213.
- Levitus, S., Burgett, R., Boyer, T.P., 1994. World Ocean Atlas, Volume 4: Temperature. NOAA, Washington D.C.
- Lichey, C., Hellmer, H.H., 2001. Modeling giant iceberg drift under the influence of sea ice in the Weddell Sea, Antarctica. *Journal of Glaciology* 47, 452–460.
- Lindsay, R., Wensnahan, M., Schweiger, A., Zhang, J., 2014. Evaluation of seven different atmospheric reanalysis products in the Arctic. *Journal of Climate* 27, 2588–2606.
- Madec, G., Imbard, M., 1996. A global mesh to overcome the North Pole singularity. *Climate Dynamics* 12, 381–388.
- Marko, J.R., Fissel, D.B., Wadhams, P., Kelly, P.M., Brown, R.D., 1994. Iceberg severity off eastern North America: its relationship to sea ice variability and climatic change. *Journal of Climate* 7, 1335–1351.
- Martin, T., Adcroft, A., 2010. Parameterizing the fresh-water flux from land ice to ocean with interactive icebergs in a coupled climate model. *Ocean Modelling* 34, 111–124.
- Marsh, R., Ivchenko, V.O., Skliris, N., Alderson, S., Bigg, G.R., Madec, G., Blaker, A., Aksenov, Y., Sinha, B., Coward, A.C., Le Sommer, J., Merino, N., Zalesny, V.B., 2015. NEMO-ICB (v1.0): interactive icebergs in the NEMO ocean model globally configured at coarse and eddy-permitting resolution. *Geoscientific Model Development* 8, 1547–1562.
- Murphy, D.L., Cass, J.L., 2012. The International Ice Patrol: safeguarding life and property at sea. Coast Guard Proceedings of the Marine Safety and Security Council 69, 13–16.
- Murray, J.E., 1967. Season of 1966. International Ice Observation and Ice Patrol Service in the North Atlantic Ocean Bulletin No. 52, CG-188-21, U.S. Coast Guard, Washington D.C.
- National Snow and Ice Data Center, 1995. Updated annually. International Ice Patrol (IIP) Iceberg Sightings Database. National Snow and Ice Data Center/World Data Center for Glaciology, Boulder, Colorado USA. Digital media.
- Newell, J.P., 1993. Exceptionally large icebergs and ice island in eastern Canadian waters: a review of sightings from 1900 to present. *Arctic* 46, 205–211.
- Orvik, K.A., Skagseth, O., Mork, M., 2001. Atlantic inflow to the Nordic Seas: current structure and volume fluxes from moored current meters, VM-ADCP and SeaSoar-CTD observations 1995–1999. *Deep-Sea Research Part I* 48, 937–957.
- Parkinson, C.L., Cavalieri, D.J., 2008. Arctic sea ice variability and trends, 1979–2006. *Journal of Geophysical Research* 113, C07003.
- Petrie, B., Buckley, J., 1996. Volume and freshwater transport of the Labrador Current in Flemish Pass. *Journal of Geophysical Research – Oceans* 101, 28335–28342.
- Reeh, N., 1985. Greenland ice sheet mass balance and sea level change. In: *Glaciers, Ice Sheets and Sea Level: Effects of a CO₂ induced Climate Change*. National Academy Press, Washington, pp. 155–171.
- Reeh, N., 1994. Calving from Greenland glaciers: observations, balance estimates of calving rates, calving laws. Workshop on the calving rate of West Greenland glaciers in response to climate change. Danish Polar Centre, Copenhagen.
- Rignot, E., Box, J.E., Burgess, E., Hanna, E., 2008. Mass balance of the Greenland ice sheet from 1958 to 2007. *Geophysical Research Letters* 35, L20502.
- Rignot, E., Velicogna, I., Van den Broeke, M.R., Monaghan, A., Lenaerts, J., 2011. Acceleration of the contribution of the Greenland and Antarctic ice sheets to sea level rise. *Geophysical Research Letters* 38, L05503.
- Rogerson, M., Colmenero-Hidalgo, E., Levine, R.C., de Abreu, L., Rohling, E.J., Voelker, A.H.L., Bigg, G.R., Schönfeld, J., Cacho, I., Siero, F.J., Löwemark, L., Reguera, M.I., de Abreu, L., Garrick, K., 2010. Enhanced Mediterranean-Atlantic exchange during Atlantic freshening phases. *Geochemistry, Geophysics, Geosystems* 11, Q08013.
- Rossby, T., Flagg, C.N., 2012. Direct measurements of volume flux in the Faroe-Shetland Channel and over the Iceland-Faroe Ridge. *Geophysical Research Letters* 39, L07602.
- Seale, A., Christoffersen, P., Mugford, R.I., O'Leary, M., 2011. Ocean forcing of the Greenland Ice Sheet: calving fronts and patterns of retreat identified by automatic satellite monitoring of eastern outlet glaciers. *Journal of Geophysical Research – Earth Surface* 116, F03013.
- Shepherd, A. et al., 2012. A reconciled estimate of ice-sheet mass balance. *Science* 338, 1183–1189.
- Straneo, F., Heimbach, P., Sergienko, O., Hamilton, G., Catania, G., Griffies, S., Hallberg, R., Jenkins, A., Joughin, I., Motyka, R., Pfeffer, W.T., Price, S.F., Rignot, E., Scambos, T., Truffer, M., Vieli, A., 2013. Challenges to understanding the dynamic response of Greenland's marine terminating glaciers to oceanic and atmospheric forcing. *Bulletin of the American Meteorological Society* 94, 1131–1144.
- Thompson, S.R., 1995. Sills of the global ocean: a compilation. *Ocean Modelling* 109, 7–9.
- Tsubouchi, T., Bacon, S., Naveira Garabato, A.C., Aksenov, Y., Laxon, S.W., Fahrbach, E., Beszczynska-Möller, A., Hansen, E., Lee, C.M., Ingvaldsen, R.B., 2012. The Arctic Ocean in summer: a quasi-synoptic inverse estimate of boundary fluxes and water mass transformation. *Journal of Geophysical Research – Oceans* 117, C01024.
- Uppala, S.M. et al., 2005. The ERA-40 re-analysis. *Quarterly Journal of the Royal Meteorological Society* 131, 2961–3012.
- Valeur, H.H., Hansen, C., Hansen, K.Q., Rasmussen, L., Thingvad, N., 1996. Weather, sea and ice conditions in eastern Baffin Bay, offshore northwest Greenland: a review. Danish Meteorological Institute Technical Report 96-12, Copenhagen.
- Van den Broeke, M., Bamber, J., Ettema, J., Rignot, E., Schrama, E., van de Berg, W.J., van Meijgaard, E., Velicogna, I., Wouters, B., 2009. Partitioning recent Greenland mass loss. *Science* 326, 984–986.
- Velicogna, I., 2009. Increasing rates of ice mass loss from the Greenland and Antarctic ice sheets revealed by GRACE. *Geophysical Research Letters* 36, L19503.
- Wadley, M.R., Bigg, G.R., 1996. Abyssal channel flow in ocean general circulation models with application to the Vema Channel. *Journal of Physical Oceanography* 26, 38–48.
- Wadley, M.R., Bigg, G.R., 1999. Implementation of variable time stepping in an ocean general circulation model. *Ocean Modelling* 1, 71–80.
- Wadley, M.R., Bigg, G.R., 2002. Impact of flow through the Canadian Archipelago and Bering Strait on the North Atlantic and Arctic circulation: an ocean modelling study. *Quarterly Journal of the Royal Meteorological Society* 128, 2187–2203.
- Webb, D.J., 1996. An Ocean model code for array processor computers. *Computational Geophysics* 22, 569–578.
- Wijffels, S., Meyers, G., 2004. An intersection of oceanic waveguides: variability in the Indonesian Throughflow region. *Journal of Physical Oceanography* 34, 1232–1253.
- Wolford, T.C., 1981. Sea ice and iceberg conditions, 1970–79. NAFO Science Council Studies 5, 39–42.
- Woodgate, R.A., Weingartner, T.J., Lindsay, R., 2012. Observed increases in Bering Strait oceanic fluxes from the Pacific to the Arctic from 2001 to 2011 and their impacts on the Arctic Ocean water column. *Geophysical Research Letters* 39, L24603.
- Wu, Y., Tang, C., Hannah, C., 2012. The circulation of eastern Canadian seas. *Progress in Oceanography* 106, 28–48.
- Zhao, Y., Bigg, G.R., Billings, S.A., Hanna, E., Sole, A.J., Wei, H., Kadirkamanathan, V., Wilton, D.J. Inferring the variation of climatic and glaciological contributions to West Greenland iceberg discharge in the Twentieth Century, Cold Regions Science and Technology (submitted for publication).